

THERMOMECHANICAL MODELING AND OPTIMIZATION OF FRICTION STIR WELDING

A Thesis

Submitted to the Graduate Faculty of the
Louisiana State University and
Agricultural and Mechanical College
in partial fulfillment of the
requirements for the degree of
Master of Science in Industrial Engineering

in

The Department of Construction Management and Industrial Engineering

by
Manthan Malde
B.E., Osmania University, Hyderabad, India, 2006
December 2009

Acknowledgments

I would like to express my sincere gratitude to Dr. T. Warren Liao, my advisor, for his invaluable guidance encouragement and support extended throughout the study.

I am thankful to the committee members, Dr. Muhammad Wahab and Dr. Pius J. Egbelu for giving their valuable time to serve in the examination committee and for their comments and inputs in my work.

I would like to thank Vinay Raghuram, Xen Xiong, Shivani Daftardar and Kranthi Kumar Charlapally for their valuable discussions on the topic.

This is a great opportunity for me to express my gratitude to my friends. I would like to thank my friends at LSU for their constant help and for making my stay at LSU memorable and enjoyable.

Thank you Kalyana, Raghava, Ravi, Varun, Sampath, Sameer, Phani, Shilpa, Hemalatha, Srilakshmi, Anuradha and Amit. I shall always remember the good times I had with you all.

I am also pleased to thank my friends Venkat, Shailey, Krishna and Sriram for their continuous support and inspiration.

I would like to thank my parents for their unconditional love, support and encouragement throughout my life. Last but certainly not the least, I would like to thank my brother and sister-in-law for their continuing concern and advice. Words cannot express how thankful I am to them for everything.

Table of Contents

Acknowledgments.....	ii
List of Tables	v
List of Figures	vi
Abstract.....	vii
1. Introduction.....	1
1.1 Background	1
1.2 Advantages and Disadvantages	3
1.3 Research Objective.....	4
2. Literature Review.....	6
2.1 On Welding Residual Stress.....	6
2.1.1 Residual Stress Measurement	6
2.2 On Modeling of Friction Stir Welding Process.....	7
2.2.1 Thermal Modeling	8
2.2.2 Thermomechanical Modeling.....	9
2.3 On Optimization of the Process	13
2.3.1 Use of Surrogate Models	15
3. Methodology Overview	17
4. Thermomechanical Model of FSW.....	19
4.1 Model Development of Friction Stir Welding for 304L Stainless Steel	19
4.2 Thermal Model.....	19
4.2.1 Assumptions.....	20
4.2.2 Geometry.....	20
4.2.3 Elements Used	20
4.2.4 Mesh Development	21
4.2.5 Material Properties.....	22
4.2.6 Boundary Condition.....	23
4.2.7 Heat Flux Input	24
4.3 Mechanical Model.....	25
4.3.1 Assumptions.....	26
4.3.2 Elements Used and Mesh Development	26
4.3.3 Plasticity Model	26
4.3.4 Boundary Conditions	28
4.4 Simulation	29
5. Validation of Thermomechanical Model of Friction Stir Welding	30
5.1.1 Temperature Responses	30
5.1.2 Stress Responses	33

6.	Parametric Study and Surrogate Models of FSW Process.....	34
6.1	Design of Experiments.....	34
6.1.1	Effect of Factors on Temperature Distribution and Residual Stress.....	35
6.2	Surrogate Models of Friction Stir Welding.....	37
6.2.1	Development of Model for Response – Temperature.....	37
6.2.2	Development of Model for Response – Residual Stress.....	38
6.3	Estimation of Performance of Developed Surrogate Models.....	39
7.	Determining Optimal FSW Parameters Using Improved Harmony Search Algorithm	42
7.1	Formulation of Optimization Problem.....	42
7.2	Solution Methodology Using Harmony Search Algorithm	44
7.2.1	Improved Harmony Search Algorithm	45
7.2.2	Pseudo Code.....	45
7.3	Optimization Results for FSW Process.....	49
7.3.1	Results for Model 1 and Model 2	49
7.3.2	Results for Model 3 and Model 4	53
8.	Validation of Optimization Results	56
9.	Conclusions and Recommendations for Future Work.....	60
	References.....	63
	Appendix A: Summary of Simulated Data	68
	Appendix B: Multiple Linear Regression Analysis	70
	B.1 Regression Model for Response Temperature Using Minitab 15	70
	B.2 Regression Model for Response Residual Stress Using Minitab 15.....	71
	Appendix C: Multiple Nonlinear Regression Analysis	72
	C.1 Regression Model for Response Temperature Using DataFit 9.0.....	72
	C.2 Regression Model for Response Residual Stress Using DataFit 9.0	72
	Vita.....	74

List of Tables

Table 4.1 Thermal material properties of 304L stainless steel	22
Table 6.1 Process parameters, range and design levels used	35
Table 6.2 Regression statistics of linear and nonlinear surrogate models	40
Table 7.1 Comparison between optimization and musical performance [59]	45
Table 7.2 Parameters used for IHS+ in this study	48
Table 7.3 Optimization results of Model 1 and Model 2 with $T_{LB} = 1000$ and $T_{UB} = 1300$	50
Table 7.4 Optimization results of Model 1 and Model 2 with $T_{LB} = 1050$ and $T_{UB} = 1150$	51
Table 7.5 Optimization results of Model 1 and Model 2 with $T_{LB} = 1140$ and $T_{UB} = 1150$	52
Table 7.6 Optimization results of Model 3 and Model 4 with constraints $T_{LB} = 1000$, $T_{UB} = 1300$ and $R_{UB} = 310$	54
Table 7.7 Optimization results of Model 3 and Model 4 with constraints $T_{LB} = 1050$, $T_{UB} = 1150$ and $R_{UB} = 310$	55
Table 8.1 Summary of results for response - temperature	56
Table 8.2 Summary of results for responses - temperature and residual stress	57

List of Figures

Figure 1.1 Friction stir welding operation principle [4]	1
Figure 3.1 Methodology of model-based optimization of FSW process	18
Figure 4.1 Three dimensional thermal solid element SOLID70 [49]	21
Figure 4.2 Three dimensional surface effect element SURF152 [49]	22
Figure 4.3 Schematic representation of boundary condition for thermal analysis	24
Figure 4.4 Temperature dependent mechanical properties of 304L stainless steel [28].....	27
Figure 4.5 Bilinear isotropic stress-strain model for 304L stainless steel	28
Figure 4.6 Flowchart of sequentially coupled thermomechanical analysis	29
Figure 5.1 Comparison of temperature distribution along the transverse direction at welding time $t= 83$ s	31
Figure 5.2 Temperature distribution on top surface of the workpiece at welding time, $t= 50.4$ sec	32
Figure 5.3 Variation of transient temperature - comparison of simulated results and results from Zhu and Chao's Model	32
Figure 5.4 Variation of the longitudinal residual stress along the traverse direction at the middle section of the workpiece.....	33
Figure 6.1 Plot of main effects for temperature	36
Figure 6.2 Plot of main effects for residual stress	36
Figure 6.3 Variation of temperature on top surface of the workpiece at different welding speeds	37
Figure 8.1 Temperature profile at $X=152.4$, $Y=0$, $Z=0$ for optimal parameters $H= 808.5$ W and $S= 2.54$ mm/s.....	57
Figure 8.2 Temperature profile at $X=152.4$, $Y=0$ m $Z=0$ for optimal parameters $H= 772.97$ W and $S= 2.312$ mm/s.....	58
Figure 8.3 Variation of the longitudinal residual stress along traverse direction operating at optimal parameters $H= 772.97$ W, $S= 2.312$ mm/s and $C= 50.2$ mm	59

Abstract

This thesis research implemented an existing thermomechanical model of friction stir welding process, and studied the surrogate model-based optimization approach to obtain optimal process parameters for the modeled friction stir welding process. As an initial step, the thermomechanical model developed by Zhu and Chao for friction stir welding of 304L stainless steel was replicated using ANSYS. The developed model was then used to conduct parametric studies to understand the effect of various input parameters like total rate of heat input, welding speed and clamping location on temperature distribution and residual stress in the workpiece. With the data from the simulated model, linear and nonlinear surrogate models were constructed using regression analysis to relate the selected input process parameters with response variables. Constrained optimization models were formulated using surrogate models and optimization of process parameters for minimizing cost and maximizing throughput was carried out using improved harmony search algorithm. To handle the constraints, Deb's parameter-less penalty method was used and implemented in the algorithm.

It is learned from this research that: (1) heat input is mainly constrained by the lower bound of the temperature for making good welds; (2) the optimal welding speed must balance the loss of heat input and the gain in productivity; (3) clamping closer to the weld is better than away from the weld in terms of lowering the peak residual stresses. Moreover, the nonlinear surrogate models resulted in a slightly better optimal solution than the linear models when wide temperature range was used. However, for tight temperature constraints, optimization on linear surrogate models produced better results. The implemented improved harmony search algorithm seems not able to converge to the best solution in every run. Nevertheless, the non-converged solution it found was very close to the best.

1. Introduction

1.1 Background

Friction Stir Welding (FSW) is a revolutionary solid state welding technique invented at The Welding Institute (TWI) in 1991 [1]. The FSW process operates below the solidus temperature of the metals being joined and hence no melting takes place during the process. This process is a derivative of the conventional friction welding and is being used to produce continuous welded seams for plate fabrication [2]. Since its invention in 1991, continuous attempts have been made by researchers to understand, use and improve this process.

Friction Stir Welding is a hot-shear joining process in which a non-consumable, rotating tool plunges into a rigidly clamped workpiece and moves along the joint to be welded [3]. The cylindrical rotating tool used in FSW has a profiled threaded or unthreaded probe of length less than the weld depth, extruding from the tool shoulder. The operating principle of FSW process is presented in figure 1.1.

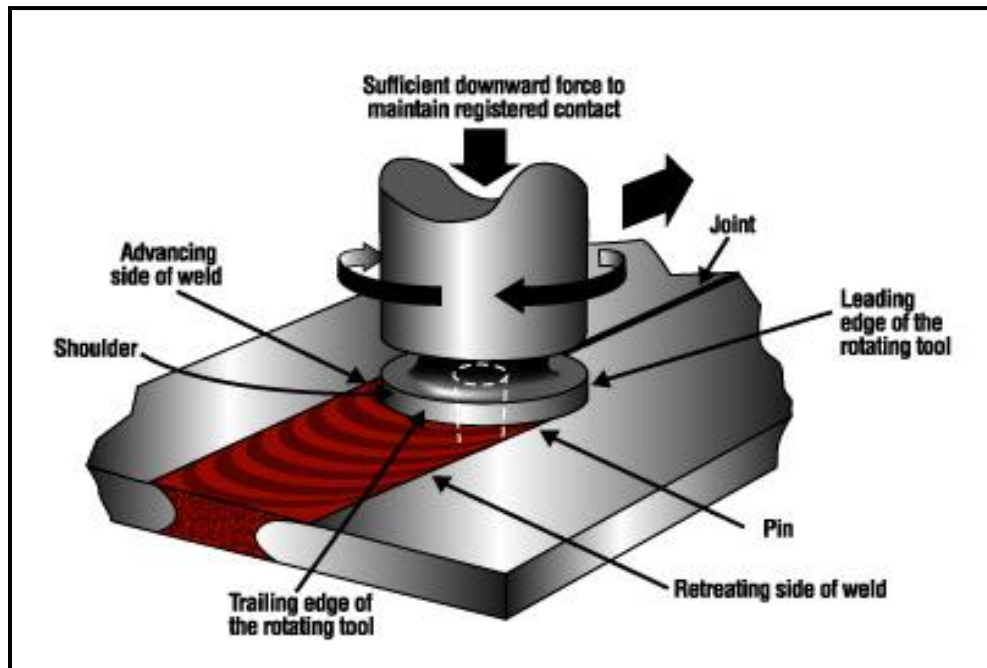


Figure 1.1 Friction stir welding operation principle [4]

The FSW process is initiated by plunging of a rotating tool into the joint until the shoulder contacts the top surface of the workpiece. As the tool translates along the joint, heat is generated by rubbing action of tool shoulder against the workpiece. Additional heat is generated by viscoplastic dissipation of mechanical energy at high strain rates due to interactions between tool and workpiece [5]. The heat thus generated results in thermal softening of the material. The thermally softened material is contained at the underside by a backing plate, at the sides by non-softened parent material, and at the top side by pin force. The softened material is then forced to flow by the translation of the tool from the front to the back of the pin where it cools, consolidates and results in joint formation [6].

FSW process requires a tool of harder material than the workpiece material being welded [2]. Previously, FSW was used for soft workpiece materials like aluminum alloys, lead, zinc, and magnesium. However, with the development of tools made from refractory material like tungsten and superabrasive materials like polycrystalline diamond (PCD) and polycrystalline cubic boron nitride (PCBN), FSW of high temperature materials was made possible [7]. As FSW process is a solid state process, it requires low heat input and it results in low distortion, no macrosegregation, and a finely recrystallised microstructure. For these reasons, FSW has been investigated for wide range of materials including high melting temperature materials such as austenitic stainless steels [8].

The feasibility of FSW for high melting temperature materials have been studied and reported. Studies have shown the feasibility of FSW in several steels and have reported that the mechanical properties of friction stir welds are comparable to those of base material [8-11]. Further, continuing investigations suggest that the FSW of steel could have several commercial applications such as pipe fabrication, rail wagons and hot plate fabrication [2, 12].

1.2 Advantages and Disadvantages

The FSW process has demonstrated a number of advantages over the conventional welding process. Some of the advantages of this thermomechanically energy efficient process are [2]:

1. The process temperatures in FSW are much lower than the fusion techniques. This results in avoiding problems which occur with liquid phase, such as alloy segregation, porosity and cracking.
2. The process can be easily automated as it is machine tool technology based.
3. High integrity similar and dissimilar welded joints are produced for an increasing range of materials – aluminum, zinc, lead, copper, magnesium, titanium and steel.
4. Reduction in production costs in further processing and finishing is possible as the surface appearance of FSW approaches to that of a rough machined surfaces.
5. No filler material or shielding gas is required.
6. The process produces lower levels of distortion in the workpiece compared to fusion welding.
7. The FSW process can be carried out in all positions – vertical and overhead. The process can also be operated underwater.
8. No special edge or joint preparation is generally required.
9. The process is environmentally friendly as no splatter, fumes or UV radiations are produced during FSW process.
10. Reduced post weld inspection and rework.

The most commonly friction stir welded steels include high strength structural steels, pipeline steels like API 5LX-100, and corrosion resistant alloys such as AISI 316L and 304L [13]. The FSW process offers advantages in terms of productivity and cost. Compared to conventional

fusion welding processes such as arc and laser beam, FSW is highly energy efficient and the estimated reduction in energy usage is by 60 to 80% [14].

Although the FSW process has many advantages, it does have some inherent disadvantages. One of the main disadvantages is that, the process requires clamping of workpiece material firmly to the base. Thus, suitable jiggling and backing bars are needed to prevent the abutting plates moving apart. This limits the portability of the process. Other problem associated with FSW is that a hole is left in the process as the probe is withdrawn. This hole is undesirable as it makes that portion of workpiece unsuitable for use. However, use of removable run-off tab can help to avoid the extract holes after the weld is completed [14]. Additionally, use of retractable pin tool has been demonstrated to overcome this problem [15].

1.3 Research Objective

Residual stresses are formed in friction stir welded workpiece. Formation of residual stresses in rigidly clamped workpiece occurs due to expansion during heating and contraction during cooling. The presence of such residual stress in a weld plate affects its distortion behavior and ability to sustain applied loads while maintaining structural integrity [3]. The study of residual stress evolution is essential in predicting the performance of the weld. Additionally, efforts have to be made to reduce the residual stresses and distortions. However, studies on residual stress in FSW steels are limited to its prediction and very few attempts have been made to investigate parameters affecting its magnitude and to optimize the thermomechanical process.

The quality of a weld joint can be assessed by its joint strength, the amount of residual stresses developed and the distortion produced. In order to achieve good quality welds, weld input parameters such as tool rotational speed, translation velocity, heat input and tool dimensions have to be properly controlled. As the quality of a weld joint is directly influenced by the input

parameters, the welding process can be considered as a multi-input, multi-output process. Thus appropriate combinations of weld parameters have to be chosen to produce high quality welds with minimum detrimental residual stresses and distortions [16]. This thesis research focuses on investigation of input parameters that control the formation of residual stresses in 304L stainless steel friction stir welds and on model-based optimization of the process.

The main objectives of this thesis are (i) to develop and validate a three dimensional thermomechanical model of FSW process and to predict the developed residual stresses, (ii) to study the effects of various process parameters on weld temperature history and residual stresses using the developed model, and (iii) to optimize FSW process with model-based approach using a traditional nonlinear optimization procedure and improved Harmony Search Algorithm.

The rest of the thesis is organized as follows: Chapter 2 reviews related works on modeling and optimization of FSW process. In chapter 3 the methodology used for achieving the set objectives is described. Chapter 4 outlines the computational approach used in the development of thermomechanical model of FSW process. Chapter 5 deals with validation of the developed thermomechanical model. Chapter 6 presents the design of experiments and results from parametric studies of the developed model. Chapter 6 also discusses the development of surrogate models for the two chosen responses, temperature and residual stress. Chapter 7 presents the formulation of optimization models and its solution using improved harmony search algorithm. Validation of optimization results are presented in chapter 8. Finally, chapter 9 presents concluding remarks and discusses the possibilities for future work.

2. Literature Review

This section has been divided into three parts. The first part outlines the techniques used for measurement of residual stresses, the second part reviews works related to thermomechanical modeling of FSW process, and the third part reviews works related to optimization of FSW process.

2.1 On Welding Residual Stress

Welding cycle often results in formation of residual stresses. The residual stresses are the locked-in stresses left out in the workpiece after the welding process is completed. The localized heating and non-uniform cooling during welding, results in a complex distribution of the residual stresses in the joint region along with undesirable deformation or distortion of the welded structure [17].

Residual stress can be beneficial or harmful depending on its compressive or tensile nature. Tensile residual stresses can cause crack initiation [3], reduce the performance or cause failure of manufactured product [18]. These tensile stresses may also increase the rate of damage by fatigue, creep or environmental degradation. On the other hand, compressive stress can lead to performance benefits [19].

2.1.1 Residual Stress Measurement

Estimation of residual stresses is usually done using measurement techniques – destructive and non-destructive techniques [3, 19].

Destructive technique involve partial destruction such as drilling a hole, sectioning a layer etc. and using specialized strain gauge rosettes to measure strain relief in the material. Some of the common destructive methods include:

1. Hole-drilling method

2. Ring core technique
3. Bending deflection method
4. Sectioning method.

On the other hand, in non-destructive techniques, measurement is carried out without destroying the weld. These techniques provide more accurate results than destructive techniques. The most commonly used techniques for non-destructive measurement include:

1. X-ray/ neutron/ synchrotron diffraction
2. Ultrasonic technique
3. Magnetic methods.

The diffraction techniques are based on using lattice spacing as strain gauge. Ultrasonic technique uses the variation of ultrasonic wave propagation in materials under the action of mechanical stress, while the magnetic methods rely on the interactions between magnetization and elastic strain in ferro-magnetic materials [19].

In recent years, with the development of powerful computing facilities, finite element analysis methods have been applied to model the welding process and to estimate residual stresses. Some of the attempts to model FSW process and estimate residual stresses are described in the following section.

2.2 On Modeling of Friction Stir Welding Process

Friction Stir Welding was invented and experimented at The Welding Institute, UK in 1991. Since then, several experimental methods, numerical/analytical and finite element methods have been developed and studied by many researchers to understand the thermal and thermomechanical interactions taking place during FSW. Despite significant advances in the FSW process, the complex thermomechanical interactions taking place have not been fully

understood. In order to predict the residual stress developed during friction stir welding, thermomechanical models are studied. In most cases, decoupled analysis was used to estimate the residual stresses. In a decoupled analysis, first pure thermal problem is solved and then the calculated temperature fields are used as input to the mechanical models.

2.2.1 Thermal Modeling

Understanding the heat generation and the temperature history during the FSW process is the first step towards understanding the thermomechanical interaction taking place during the welding process. The initial modeling approaches focused on approximate estimation of heat generated during the FSW process. Gould and Feng [20] developed a preliminary thermal model to predict the temperatures of friction stir welds using the Rosenthal equations to describe a moving heat source. The heat input was described as a function of process parameters such as tool rpm and force on tool.

Chao, Qi and Tang [21] formulated a boundary value problem for tool and workpiece in order to study the heat transfer in friction stir welding. They determined the frictional heat flux from the measured transient temperature fields obtained in the finite element analyses. In an attempt to predict the flow of material around the tool, Colegrove *et al.* [22] presented a finite element based thermal model of FSW. Their model included the backing plate and the tool. In their work, the heat input was fitted through iterative process for verification between the modeled and experimental values.

An input torque based thermal model for prediction of temperature in friction stir welds of Al-6061-T6 alloy was developed by Khandkar *et al* [23]. In their model, the heat generated by tool rotation and linear traverse of shoulder and pin, has been correlated with actual machine power input. This estimated heat was applied as a moving heat to obtain the temperature distribution

across the weld.

The above mentioned models did not include the tool penetration and pulling out phase. Song and Kovacevic [24] proposed a coupled heat transfer model of both the tool and the workpiece for FSW to include the tool penetration and pulling out phase. A moving coordinate was adopted to reduce the difficulty of modeling the heat generation due to the movement of the tool pin. The finite difference method was used for solving the control equations and the results obtained were in good agreement with the experimental results.

Vilaca *et al.* [25] developed an analytical thermal model for simulation of friction stir welding process. The model included simulation of the asymmetric heat field under the tool shoulder resulting from viscous and interfacial friction dissipation. The analytical model also considered the influence of hot and cold FSW conditions into the heat flow around the tool.

The focus of all the thermal models was to understand the process of heat generation and to predict the temperature distribution in the workpiece and tool. A thermal model forms the basis for the development of mechanical and microstructural models.

2.2.2 Thermomechanical Modeling

In order to estimate residual stress and distortions in workpiece resulting from welding process, thermomechanical models were developed and studied. One of the first thermomechanical models for FSW was studied by Chao and Qi [26]. A decoupled heat transfer and a subsequent thermomechanical analysis for Al 6061-T6 was used in their study. Heat generated from friction between tool shoulder and workpiece was implemented as the heat input. The empirical equation for calculating the heat input to the workpiece is given by equation (2.1).

$$q(r) = \frac{3Qr}{2\pi(r_o^3 - r_i^3)} \quad \text{for } r_i \leq r \leq r_o \quad (2.1)$$

where $q(r)$ is the rate of heat input, r_o and r_i are the radii of the shoulder and the nib of the pin tool, and Q is the total rate of heat input to the workpiece expressed as shown in equation (2.2).

$$Q = \frac{\pi\omega\mu F(r_o^2 + r_o r_i + r_i^2)}{45(r_o + r_i)} \quad (2.2)$$

where, ω is the tool rotational speed, μ is the frictional coefficient, and F is the downward force. The total heat input and heat transfer coefficient were estimated by fitting the measured temperature data with the analytical model by a trial and error approach. The temperatures thus obtained from the analysis were used to determine the residual stress retained in the friction stir welds. The maximum residual stresses were reported to be 30% of the yield strength of the material.

Chen and Kovacevic [27] proposed a three dimensional finite element analysis model to study the thermal history and thermomechanical process in butt welding of aluminum alloy 6061-T6. The model incorporated the mechanical reaction of the tool and thermomechanical processes of the welded material. The friction between the material, the probe and the shoulder was included in the heat source. X-ray diffraction technique was used to measure the residual stresses developed in the plate and the measured results were used to validate the efficiency of the proposed model. From the study, it was reported that fixturing release to the welded plates affected the stress distribution of the weld.

Zhu and Chao [28] presented three-dimensional nonlinear thermal and thermomechanical simulations using finite element analysis code –WELDSIM on 304L stainless steel friction stir welded plates. Initially, a heat transfer problem was formulated as a standard boundary value problem and was solved using the inverse analysis approach. The total heat input and heat transfer coefficient were estimated by fitting the measured temperature data with the analytical model. Later, the transient temperature outputs from the first stage were used to determine

residual stresses in the welded plates using a three-dimensional elastic plastic thermomechanical model. Convection and radiation were assumed to be responsible for heat loss to the ambient on the surface. Their model provided good match between experimental and predicted results. They reported that the residual stress in the welds after fixture release decreased significantly as compared to those before fixture release. They also reported that about 50% of the total mechanical energy developed by FSW machine was utilized in raising the temperature of the workpiece.

Soundararajan *et al.* [29] developed a finite element thermomechanical model with mechanical tool loading considering a uniform value for contact conductance and used for predicting the stress at workpiece and backing plate interface. The non-uniform contact conductance were defined from pressure distribution contours and used in predicting the temperatures in the thermal model. The thermomechanical model was then used in predicting the developed stresses. Khandkar *et al.* [30] developed coupled finite element models to predict residual stress in AA-2024, AA-6061 and SS 304L friction stir welds. In their models, the temperature history predicted by the thermal model was sequentially coupled to a mechanical model to assess the residual thermal stresses developed during the welding. It was found that clamping constraints and their locations had significant localized effects on the stress components in the unaffected base metal beyond the heat-affected zone.

Feng *et al.* [31] presented a more detailed thermal-metallurgical-mechanical model to study the microstructure changes and their effects on residual stress distribution in friction stir weld of Al6061-T6. In their approach, the first stage involved a transient nonlinear heat flow analysis to determine the temperature distribution. The frictional heating in the thin layer near the interface was treated as a surface heat generation term, q , which was estimated by the equation (2.3).

$$q = \frac{2\eta\mu F\omega}{60(R_{sh}^2 - R_{pin}^2)} r \quad \text{for } R_{pin} \leq r \leq R_{sh} \quad (2.3)$$

where F is the downward force, ω is the rotational speed, η is the process efficiency, μ is the interpretive coefficient of friction, and R_{pin} and R_{sh} the radii of the pin and the shoulder respectively. In the second stage, using the temperature history from the thermal model as input, the metallurgical calculations were performed in the mechanical analysis as a part of material constitutive definition subroutine. It was reported that residual stresses had strong dependence on the welding speed.

Li *et al.* [32] presented a semicoupled thermomechanical finite element model containing both thermal load and mechanical load. Their model included an autoadapting heat source in the thermal model and fixtures were included in the mechanical model. They reported that in the case of 2024-T6 alloy, stresses at the retreating side of the weld were smaller than those at the advancing side.

Bastier *et al.* [33] used computational fluid dynamics package to estimate the material flow and temperature field in 7050 aluminum alloy. They used the results to estimate residual state induced in friction stir welding process based on elasto-viscoplastic constitutive law. They also reported from the parametric study that the welding speed and rotational speed had influence on the level of residual stresses and distortions developed during welding.

Some researchers conducted experimental studies to investigate the effect of process parameters on the residual stresses. Peel *et al.* [34] investigated the microstructure, mechanical properties and residual stress as a function of welding speed for AA5083 friction stir welds. They reported that the weld properties were characterized by thermal input rather than the mechanical deformation by the tool. They also reported that with the increase in traverse speed the weld zone

decreases, while the peak longitudinal stress increases.

Staron *et al.* [35] conducted experimental study on residual stress states in FSW joints in 6.3 and 3.2 mm thick AA2024 sheets that had been welded under mechanical tensioning. They were successful in reducing the tensile residual stress in the weld zone by induction of large compressive stresses through mechanical tensioning.

Dattoma *et al.* [36] evaluated the residual stress fields in similar and dissimilar joints in 2024-T3 and 6082-T6 Aluminum alloy using hole-drill method. Findings from their study showed that in thicker joints very high longitudinal stresses were present and adequate shoulder geometries resulted in reduction of residual stress values.

2.3 On Optimization of the Process

Optimization is an iterative process of finding the optimal parameters without violating the set constraints. Friction stir welding process operation in general can also be optimized by obtaining optimal values for parameters such as tool rotational speed, axial force, traverse speed, tool dimension and other such parameters. Several optimization techniques could be applied to optimize FSW models. However, as the FSW is relatively new technology, there have been only a few attempts to use mathematical optimization techniques to optimize the process. Some of the mathematical optimization techniques applied to FSW have been summarized in the following paragraphs.

Squillac *et al.* [37] investigated the effect of rotational and welding speed on tensile strength and fatigue strength of AA 6056 joints made by FSW. The influence of process parameters on the weld quality was assessed by Analysis of Variance (ANOVA) methods using the experimental results. A complete two factor factorial experiment, with three replicates was performed by the authors.

Meng *et al.* [38] used a multi-targeted optimization with constraint based on genetic algorithm for optimization of stir head dimensions. The objective function employed was an analytically derived mathematical model relating heat input coefficient with tool parameters. The goal of optimization was to determine the shoulder diameter and pin diameter of the stirring tool for maximizing the tensile strength of the friction stir welds of aluminum-lithium alloy.

In addition to design of experiment techniques, some evolutionary algorithms were utilized for optimization of FSW. Fratini and Corona [39] investigated FSW lap joint resistance optimization using gradient techniques. They combined the gradient technique and the finite difference method to determine the optimal rotating speed and welding speed in order to maximize the joint strength per unit length.

Nandan *et al.* [40] used genetic algorithm to determine four process parameters by minimizing the difference between the numerical model and experiments. The process parameters included variable friction coefficient, the extent of sticking, the heat transfer coefficient, and the extent of viscous dissipation converted into heat. These selected parameters were optimized by a genetic algorithm using a limited volume of measured temperatures at several monitoring locations during FSW of dissimilar aluminum alloys AA 1200 and AA 6061.

Use of Artificial neural network (ANN) was proposed by Okuyucu *et al.* [41] to obtain correlation between FSW parameters and mechanical properties of aluminum plates. Their attempt was to correlate the parameters rather than to optimize them. The input parameters were weld speed and tool rotational speed while the output parameters included mechanical properties such as tensile strength, elongation, hardness of weld metal and hardness of heat affected zone. The obtained model was used to calculate mechanical properties of welded Al plates as a function of weld speed and rotational speed.

Conventional parametric design of experimental approach is cumbersome and requires large number of experimental trials. Statistical techniques are often used to reduce the number of experiments conducted. Lakshminarayanan *et al.* [42] used one such statistical technique known as Taguchi technique to determine the effect of three process parameters, i.e. tool rotational speed, traverse speed, and axial force on the tensile strength of friction stir welded RDE-40 aluminum alloy. Jayaraman *et al.* [43] used a similar technique to find the effect of three process parameters on the tensile strength of friction stir welded A319 aluminum alloy. In both these studies, the authors performed Analysis of Variance (ANOVA) to identify statistically significant process parameters.

2.3.1 Use of Surrogate Models

Some techniques such as surrogate model or meta-model based optimization have been used in optimization. The benefit of using surrogates in optimization is that a fast approximate model instead of a computationally expensive model can be used to speed up the optimization process [44].

Elangovan *et al.* [45] developed a mathematical model using response surface method (RSM) to develop relationship between four process parameters and tensile strength for AA6061. The process parameters included tool rotational speed, welding speed, axial force and the tool pin profile. A similar study was carried out by Babu *et al.* [46] but on a different aluminum alloy AA2219. Both the studies used Hooke and Jeeves search algorithm to achieve maximum tensile strength. Both the studies reported close match between the optimized values and the experimentally determined values.

More recently, Liao and Daftardar [47] proposed a model-based approach for optimization of FSW process for AA2195-T8. They developed two surrogate models from thermal model to

relate three process parameters such as heat input, welding speed and shoulder diameter with maximum temperature at selected location. Further, a constrained optimization model was formulated and solved using five population-based metaheuristics to find the optimal solutions. The performance of different metaheuristics was evaluated and it was reported that differential evolution technique had the best performance.

3. Methodology Overview

To accomplish the research objectives set forth for this study, a methodology was developed. The methodology was essentially a model-based approach for optimization of FSW process. The first task was to develop and validate a thermomechanical model of FSW process in consideration of various published papers as discussed in literature review. The model chosen for this task was the thermomechanical model developed by Zhu and Chao [28] for FSW of 304L stainless steel. The thermomechanical model was developed using commercial finite element analysis program ANSYS® -11.0. In order to validate the developed model, the output of the model was correlated with the published results. Once developed, the thermomechanical model was used to simulate the process. The model was then extrapolated to perform parametric studies in order to investigate effects of various process parameters on temperature distribution and residual stress in the workpiece.

The next step was to construct surrogate models using the data generated by the thermomechanical model. Linear and nonlinear surrogate models were constructed to relate process parameters with responses, i.e., temperature and residual stress measured at selected location. The performance of the developed surrogate models was estimated using several statistical measures. In the next step, constrained optimization models were formulated with goal of maximizing throughput and minimizing manufacturing costs. The optimization models were solved using a traditional nonlinear optimization procedure and a population-based metaheuristics, improved harmony search algorithm. Finally, the optimal results were validated by simulation using ANSYS®. Figure 3.1 presents an overall methodology of surrogate model-based optimization of friction stir welding process.

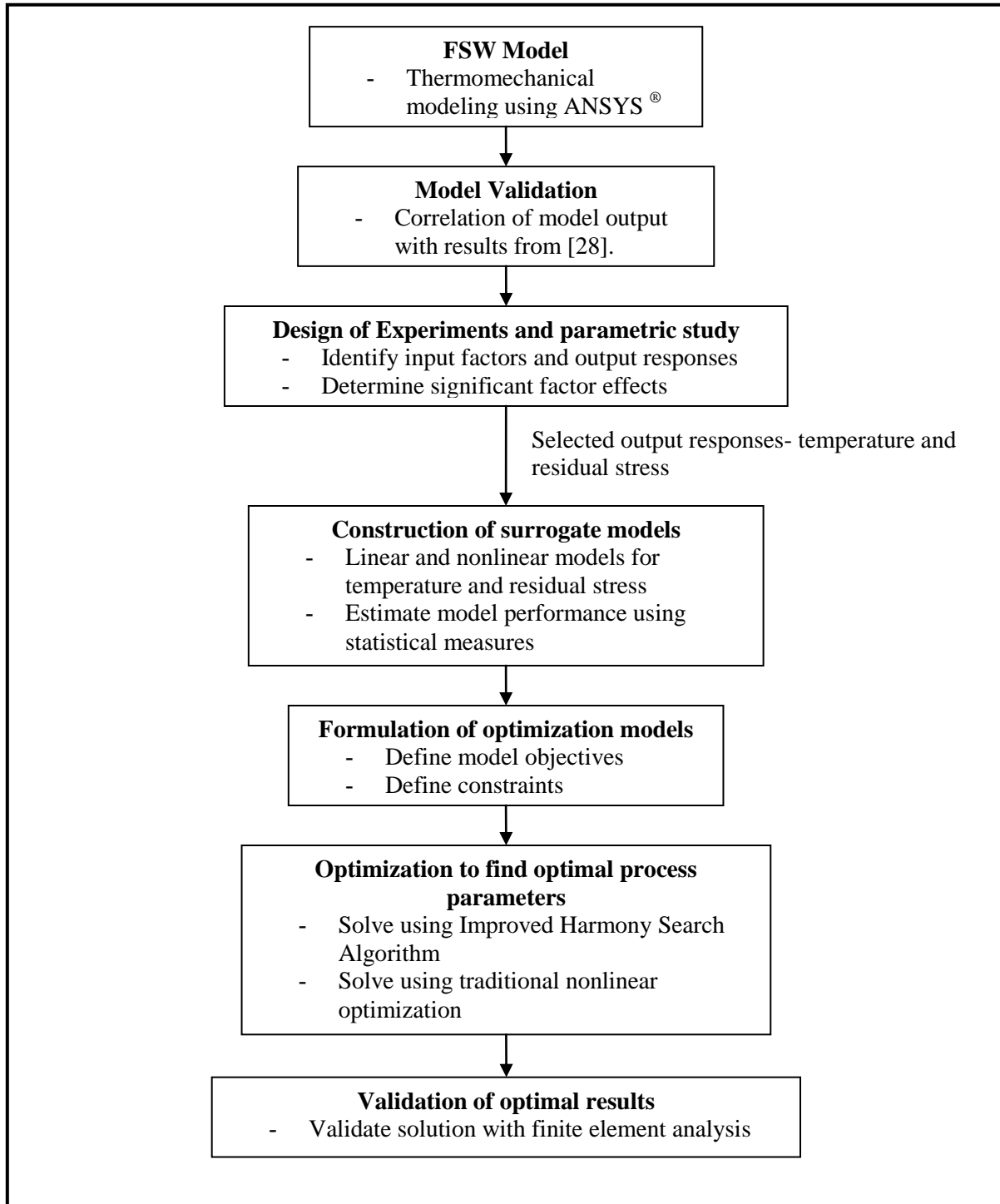


Figure 3.1 Methodology of model-based optimization of FSW process

4. Thermomechanical Model of FSW

4.1 Model Development of Friction Stir Welding for 304L Stainless Steel

The Finite Element Method (FEM) offers a way to solve complex continuum problems by subdividing it into a series of simple interrelated problems. FEM is most commonly used in numerical analysis for obtaining approximate solutions to wide variety of engineering problems [48]. In the present study, a commercial general purpose finite element program ANSYS® 11.0 was used for numerical simulation of friction stir welding process.

The ANSYS® program has many finite element analysis capabilities, ranging from simple, linear, static analysis to a complex nonlinear, transient dynamic analysis [49]. The thermal and mechanical responses of the material during friction stir welding process are investigated by finite element simulations. In this study, a sequentially coupled thermomechanical model is developed for analysis. First, a nonlinear, transient three-dimensional heat transfer model is developed to determine the temperature fields. Later, the temperature fields are used as input for a nonlinear, rate independent, three-dimensional structural model in order to predict the distortions and the residual stresses. The finite element models are parametrically built using APDL (ANSYS Parametric Design Language) provided by ANSYS® [49]. The models are then validated by comparing the results with established numerical data.

4.2 Thermal Model

The purpose of the thermal model is to calculate the transient temperature fields developed in the workpiece during friction stir welding. In the thermal analysis, the transient temperature field T which is a function of time t and the spatial coordinates (x, y, z) , is estimated by the three dimensional nonlinear heat transfer equation (4.1).

$$k \left(\frac{\partial^2 T}{\partial x^2} + \frac{\partial^2 T}{\partial y^2} + \frac{\partial^2 T}{\partial z^2} \right) + Q_{int} = c\rho \frac{\partial T}{\partial t} \quad (4.1)$$

where k is the coefficient of thermal conductivity, Q_{int} is the internal heat source rate, c is the mass-specific heat capacity, and ρ is the density of the materials [28,50]. The heat transfer model developed for the thermal analysis is described in the following section.

4.2.1 Assumptions

A number of assumptions have been made in developing the finite element thermal model, which include:

- Workpiece material is isotropic and homogeneous.
- No melting occurs during the welding process.
- Thermal boundary conditions are symmetrical across the weld centerline.
- Heat transfer from the workpiece to the clamp is negligible.

4.2.2 Geometry

In the numerical model, only half of the welded plate is modeled as the weld line is the symmetric line. Symmetric condition is used to reduce the simulation time. The workpiece has dimensions of 0.3048 m x 0.1016 m x 0.00318 m.

4.2.3 Elements Used

In the present thermal analysis, the workpiece is meshed using a brick element called SOLID70. This element has a three-dimension thermal conduction capability and can be used for a three-dimensional, steady-state or transient thermal analysis [49]. The element is defined by eight nodes with temperature as single degree of freedom at each node and by the orthotropic material properties. Heat fluxes or convections (but not both) can be input as surface loads at the element

faces as shown by the circled numbers on the element geometry in Figure 4.1. An advantage of using this element is that, the element can be replaced by an equivalent structural element for the structural analysis.

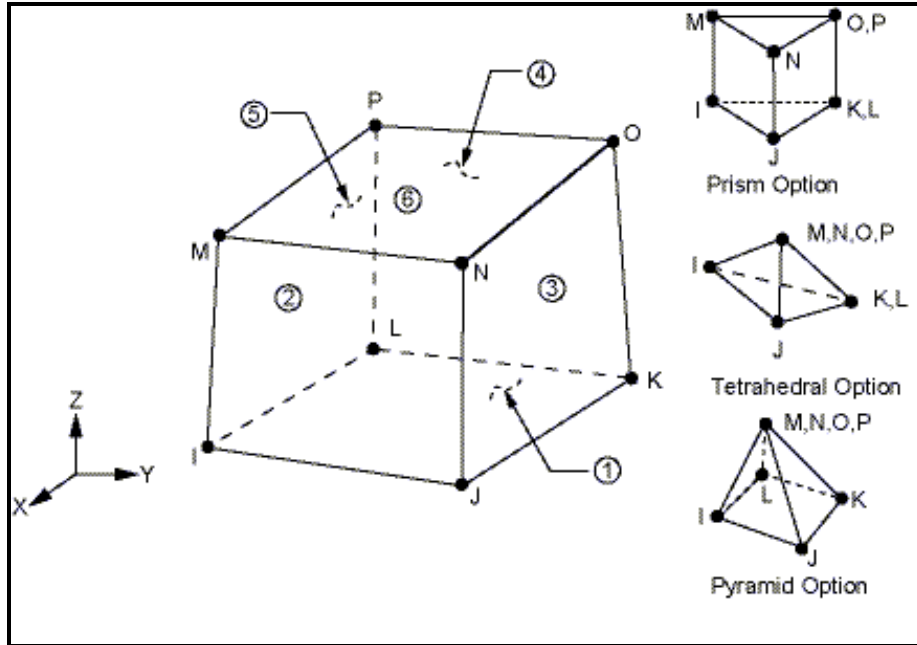


Figure 4.1 Three dimensional thermal solid element SOLID70 [49]

As SOLID70 cannot apply heat flux and convection at the same time, a three-dimensional thermal-surface-effect element was used. For applying convection on the workpiece surface, SURF152 was used overlaying it onto faces of the base elements made by SOLID70. The convections were applied as a surface load by choosing KEYOPT (8) >1. Figure 4.2 shows the geometry, node locations, and the coordinate system of the element, which is defined by four to nine nodes and the material properties.

4.2.4 Mesh Development

Three dimensional SOLID70 elements were used to mesh the sheets. The workpiece was divided into 100 parts along the length, 40 parts along the width and 2 parts along the thickness direction. The mesh is comprised of a total number of 8000 elements.

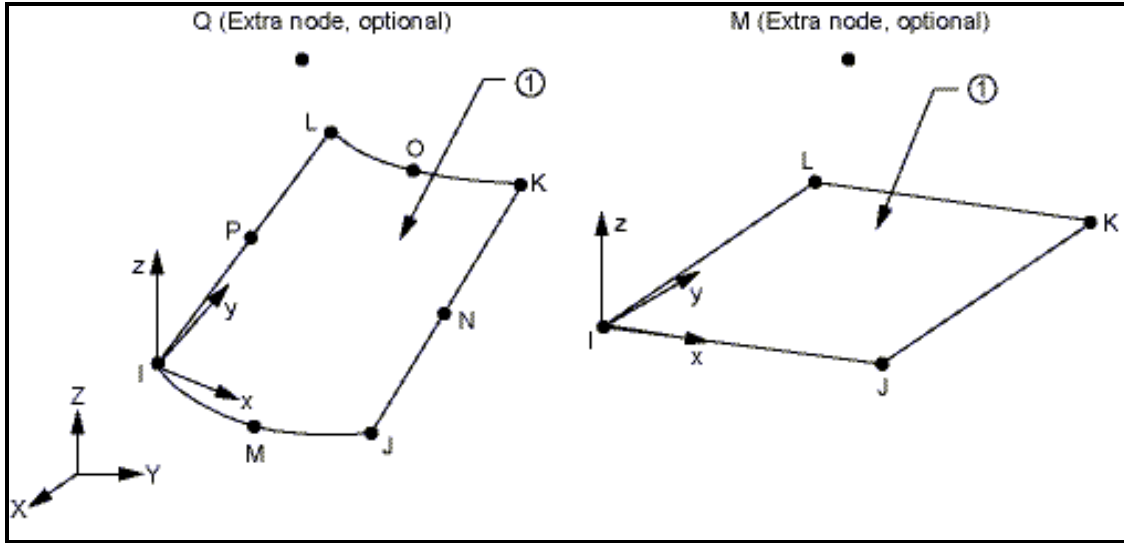


Figure 4.2 Three dimensional surface effect element SURF152 [49]

4.2.5 Material Properties

Thermal properties of the material such as thermal conductivity, specific heat, and density are temperature dependent. An accurate estimation of temperatures is critical in FSW process because the stresses and strains developed in the weld are temperature dependent. Therefore, temperature dependent thermal properties of 304L steel are used in finite element model.

The thermal material properties of 304L stainless steel are tabulated in Table 4.1. The thermal property values are obtained from [28, 51], and for higher temperatures the values are linearly extrapolated.

Table 4.1 Thermal material properties of 304L stainless steel

Temperature (°C)	0	200	400	600	800	1000
Specific heat (J/kg °C)	484	541	563	586	593	593
Thermal Conductivity (W/m °C)	14.2	16.9	20.6	23.3	27.8	27.8
Density (Kg/m ³)	7894	7744	7631	7518	7406	7406

In order to define the temperature dependent properties, combination of MPTEMP and MPDATA commands was used. MPTEMP was used to define a series of temperatures, and later MPDATA was used to define corresponding material property values.

4.2.6 Boundary Condition

Boundary condition for FSW thermal model were specified as surface loads through ANSYS® codes. Assumptions were made for various boundary conditions based on data collected from various published research papers [28, 30, 52].

Convective and radiative heat losses to the ambient occurs across all free surfaces of the workpiece and conduction losses occur from the workpiece bottom surface to the backing plate. To consider convection and radiation on all workpiece surfaces except for the bottom, the heat loss q_s is calculated by equation (4.2).

$$q_s = \beta(T - T_0) + \varepsilon\sigma(T^4 - T_0^4) \quad (4.2)$$

where T is absolute temperature of the workpiece, T_0 is the ambient temperature, β is the convection coefficient, ε is the emissivity of the plate surfaces, and $\sigma = 5.67 \times 10^{-12} \text{ W/cm}^2\text{°C}$ is the Stefan-Boltzmann constant. In the current model, a typical value of β was taken to be $10 \text{ W/m}^2\text{°C}$ using an ambient temperature of 300 K and ε was taken to be 0.17 for 304L steel.

In order to account for the conductive heat loss through the bottom surface of weld plates, a high overall heat transfer coefficient has been assumed. This assumption is based on the previous studies [21, 28]. The heat loss was modeled approximately by using heat flux loss by convection q_b given by equation (4.3).

$$q_b = \beta_b(T - T_0) \quad (4.3)$$

where β_b is a fictitious convection coefficient. Due to the complexity involved in estimating the contact condition between the sheet and the backing plate, the value of β_b had to be estimated

by assuming different values through reverse analysis approach. In this study, the optimized value of β_b was found to be $100 \text{ W/cm}^2\text{°C}$. Figure 4.3 shows the schematic representation of boundary conditions that were used for thermal analysis

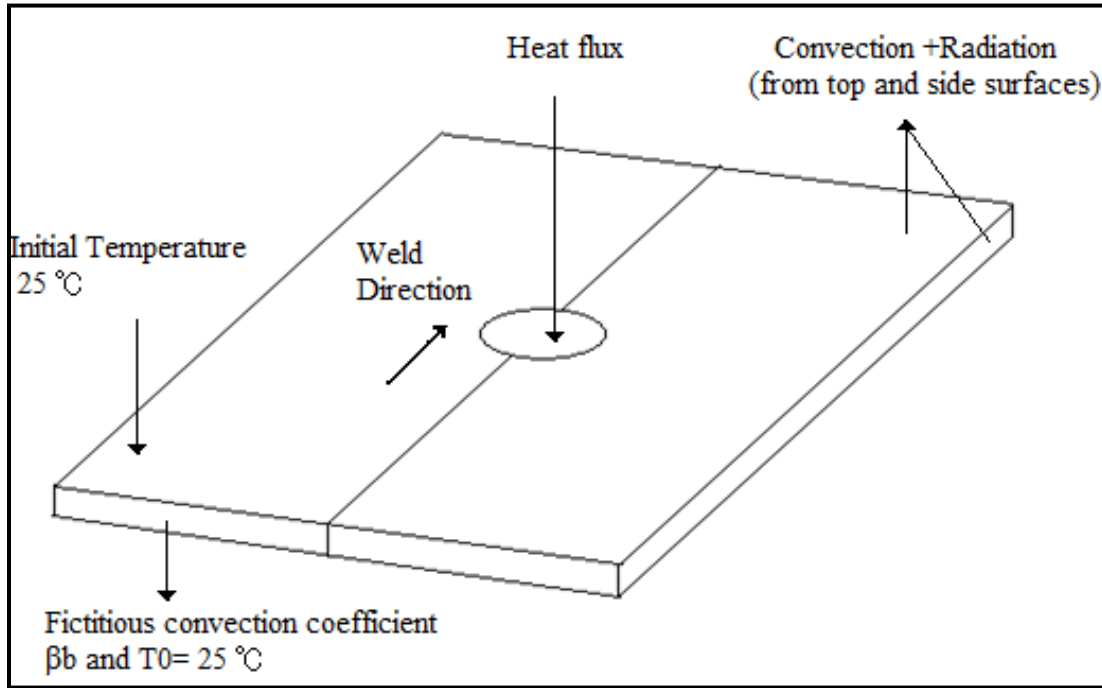


Figure 4.3 Schematic representation of boundary condition for thermal analysis

4.2.7 Heat Flux Input

Heat is produced in the friction stir welding process due to the friction between the tool shoulder and workpiece interface and due to the plastic deformation of the weld metal near the pin. The heat generated by the plastic deformation of weld metal near the pin is of negligible magnitude and is difficult to quantify [21, 53, 54]. Hence, it was neglected in this study. Therefore in this model, the heat generated by friction between the workpiece and tool shoulder is the only source of heat generation.

The total heat input Q in watts for this model is calculated through Chao *et al.* [21] equation and is applied as a moving heat flux. The total heat input Q is given by equation (4.4).

$$Q = \frac{\pi\omega\mu F(r_o^2 + r_o r_i + r_i^2)}{45(r_o + r_i)} \quad (4.4)$$

where ω is the tool rotational speed, μ is the frictional coefficient, F is the downward force, and r_o and r_i are the radii of the shoulder and the nib of the pin tool.

The rate of heat input to the workpiece $q(r)$ is assumed to be axis-symmetric and linearly distributed in the radial direction [21] and is calculated by equation (4.5).

$$q(r) = \frac{3Qr}{2\pi(r_o^3 - r_i^3)} \quad \text{for } r_i \leq r \leq r_o \quad (4.5)$$

In the present simulation, the heat flux $q(r)$ obtained from the equation (4.5) is applied as surface load using tabular boundary condition. The movement of FSW tool is implemented by creating a local cylindrical coordinate system and calculating heat load at each node at each instantaneous time step.

The dimensions for tool and values for other parameters used in this study were obtained from Zhu and Chao [28] for correlation to the published research data. The tool shoulder diameter used in this study was 19.05 mm, while the pin diameter was assumed as zero. The assumption was made based on findings from Russell and Sheercliff [55] that the heat generated at the pin of the tool is in the order of 2% of total heat and hence negligible. Fitted values of Q and β_b were used in this study. For the verification of the model, values of heat input $Q = 760$ watts and $\beta_b = 100 \text{ W/cm}^2\text{°C}$ for 300 rpm were used.

4.3 Mechanical Model

The second step in the thermomechanical analysis is development of the mechanical model. The temperature distributions obtained from the thermal analysis are used as input to the mechanical model. This model is used to estimate the weld induced residual stresses. The mechanical model developed for the analysis is described in this section.

4.3.1 Assumptions

The following assumptions have been made in developing the structural model:

- Deformation occurs symmetrically along the weld line, so only half of the workpiece is modeled.
- The plate material is homogeneous.
- The effect of creep is neglected because there is no cyclic thermal load involved.

4.3.2 Elements Used and Mesh Development

A structural element defined by eight nodes (i.e., SOLID185) having three degrees of freedom at each node is used for the modeling of plate. This element supports plasticity, hyperelasticity, stress stiffening, creep, large deflection, and large strain capabilities [49].

In the present analysis, the heat transfer model containing the equivalent thermal element SOLID70 is replaced by SOLID185 by switching the element type from thermal to structural using the command ETCHG. The advantage of using this element type is that the temperatures obtained from thermal step can be applied as element body loads at the nodes. The geometry, node locations, and the coordinate of this element are equal to those of SOLID70 element. An identical mesh pattern generated for the thermal analysis is used in the structural analysis.

4.3.3 Plasticity Model

Plastic behavior involved in friction stir welding process begins when the induced stress exceeds the yield point of the material. The plasticity is characterized by nonlinear relationship between stress and strain. The plasticity model is defined by three essential principles – a yield criterion, a flow rule and a hardening rule [49]. A yield criterion determines the stress level at which yielding is initiated, a flow rule relates the applied stress increments to the resulting plastic strain

increments once plastic flow has begun, and a hardening rule describes the change in the yield criteria as a function of plastic strains [49,56].

In the present thermomechanical analysis, the incremental theory of plasticity is employed. The plastic deformation of the material is assumed to obey von Mises yield criterion, the associated flow rule and the work hardening rule. This assumption is made based on the assumption made by Zhu and Chao [28] in their study. Accordingly, a bilinear isotropic hardening model (BISO), provided by ANSYS[®] software is used. A BISO model incorporates von Mises yield criteria, and associated flow rules coupled with isotropic work hardening rule. In the model, the stress-strain behavior is described by bilinear stress-strain curves. Figure 4.4 presents the yield stress, Young's modulus and thermal expansion coefficient of 304L stainless steel at various temperatures. A constant plastic modulus of 2.8 GPa is used in all calculations to consider the effect of strain hardening on the residual stresses. Figure 4.5 shows the stress-strain behavior of bilinear isotropic material used in the analysis.

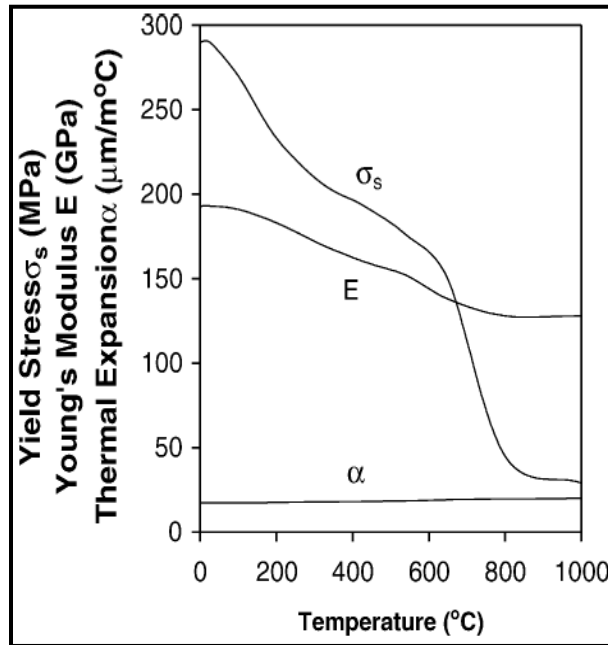


Figure 4.4 Temperature dependent mechanical properties of 304L stainless steel [28]

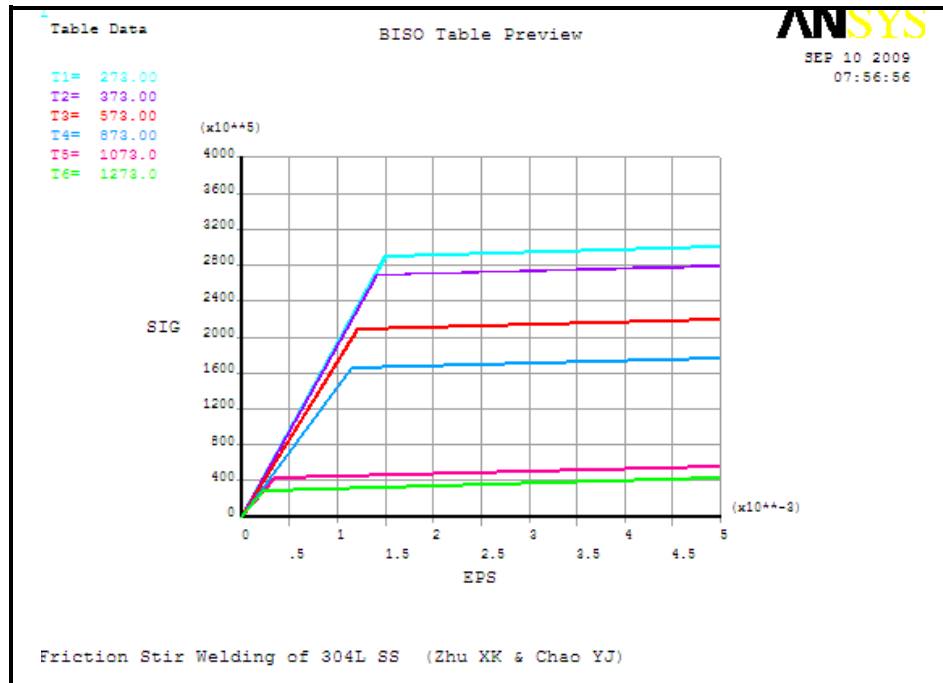


Figure 4.5 Bilinear isotropic stress-strain model for 304L stainless steel

4.3.4 Boundary Conditions

In the present analysis, sequentially coupled finite element analysis is carried out. The temperature histories obtained from thermal analysis are applied as body loads in the mechanical analysis. The forces from the thermal expansion of the workpiece material are the only forces considered in this analysis.

The following boundary conditions are utilized for the mechanical analysis:

- The workpiece is constrained of vertical motion at the bottom surface.
- The workpiece is fixed through clamping by 304.8 mm long L-shaped steel strip (25.4 mm x 25.4 mm x 6.35 mm) on each plate at a distance 50.8 mm from the weld center. Totally rigid boundary conditions are applied at these clamping locations. The clamping constraints are released after the weld cools down to room temperature.
- There are no displacements along the symmetric surface.

4.4 Simulation

The thermomechanical modeling was carried out in two stages. Transient thermal analysis is the first stage followed by nonlinear transient structural analysis in the second stage. Figure 4.6 illustrates the flow diagram of the method used for the finite element analysis. Since the problem involves nonlinear analysis, full Newton-Raphson option was used to solve the nonlinear equations.

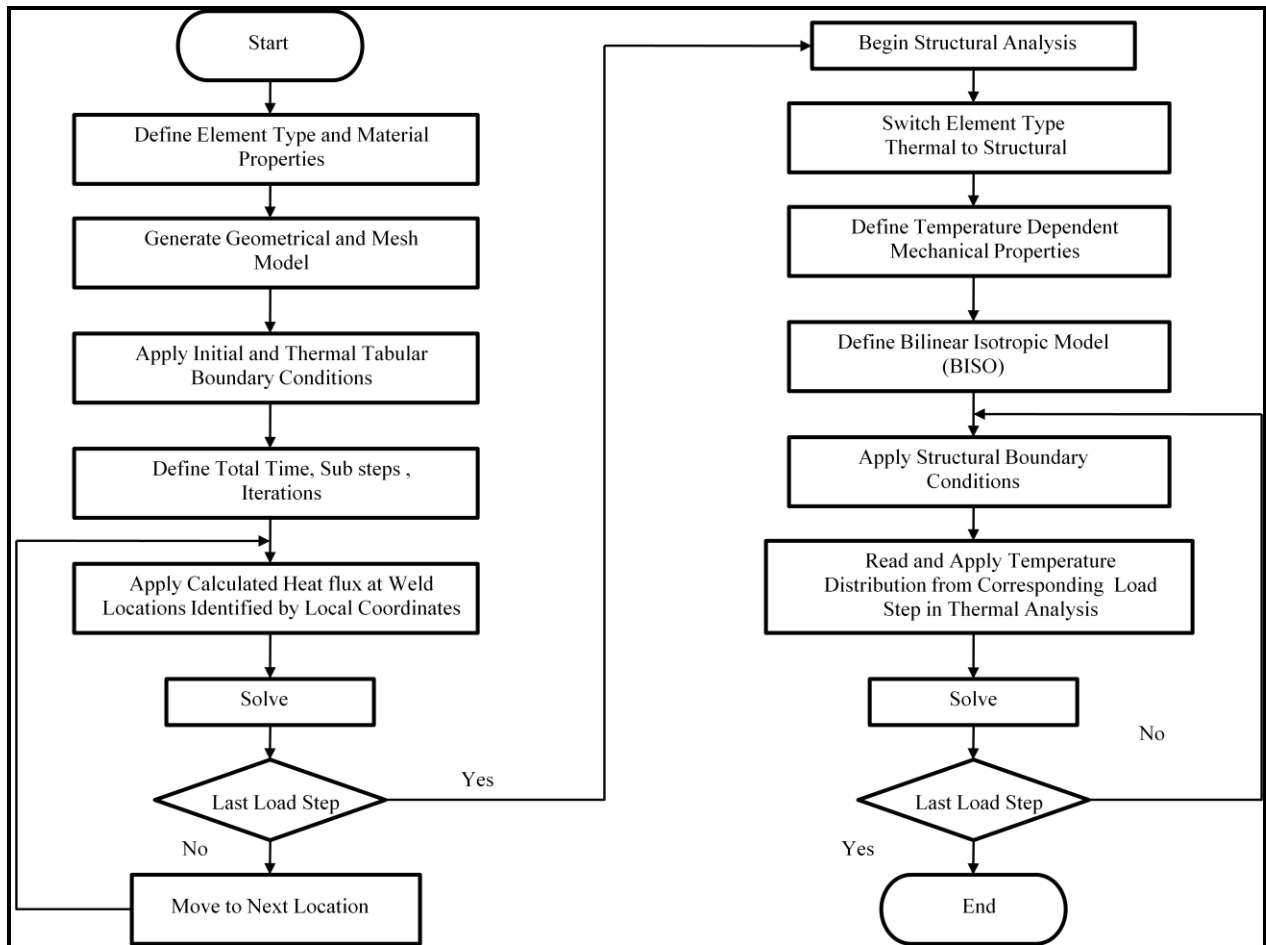


Figure 4.6 Flowchart of sequentially coupled thermomechanical analysis

5. Validation of Thermomechanical Model of Friction Stir Welding

For validating the thermomechanical model developed using ANSYS®, it was essential to correlate the developed model with the published results. For this purpose, the developed thermomechanical model was verified with numerical results obtained by Zhu and Chao [28].

The model used for validation had dimension of 304.8 mm x 101.6 mm x 3.18 mm of 304L stainless steel material. The tool shoulder diameter was 19.05 mm and the tool pin diameter was 6.35 mm. The tool rotational speed was 300 rpm and the applied downward force was 31.1 KN. The welding was assumed to start at a location 6.4 mm away from the edge of the workpiece and stop after translation of 279.4 mm along the weld line with a velocity of 1.693 mm/s.

It was difficult to predict the values for the convective heat transfer coefficient at bottom surface and the total rate of heat input. Zhu and Chao [28] conducted inverse analysis to fit the values of these two uncertain parameters with maximum temperature measured during FSW experiments. To correlate the model to existing numerical data, fitted values of Q and β_b are used in this study. A convection coefficient of $100 \text{ W/m}^2\text{°C}$ was applied at the bottom surface of the workpiece. The heat input of 760 W was applied as a moving heat flux along the weld line. Additionally, a convection coefficient of $10 \text{ W/m}^2\text{°C}$ was applied at all the surfaces except the bottom surface.

5.1.1 Temperature Responses

Measurement of temperature was made by Zhu and Chao [28] through the use of 36 gauge K-type thermocouples embedded at nine locations on the top and bottom surface along the transverse section of the workpiece. The graph in figure 5.1 shows the comparison of instantaneous experimental and simulation results for top surface of workpiece. The workpiece temperature were measured and calculated along the traverse direction of weld line at $t= 83$

seconds, i.e., at a distance of 152.4 mm from the edge of the workpiece. From the figure 5.1, it is seen that the highest temperature during the welding is distributed within the shoulder region and has the value between 900 and 1150°C. This range is lower than the melting temperature of 304L stainless steel.

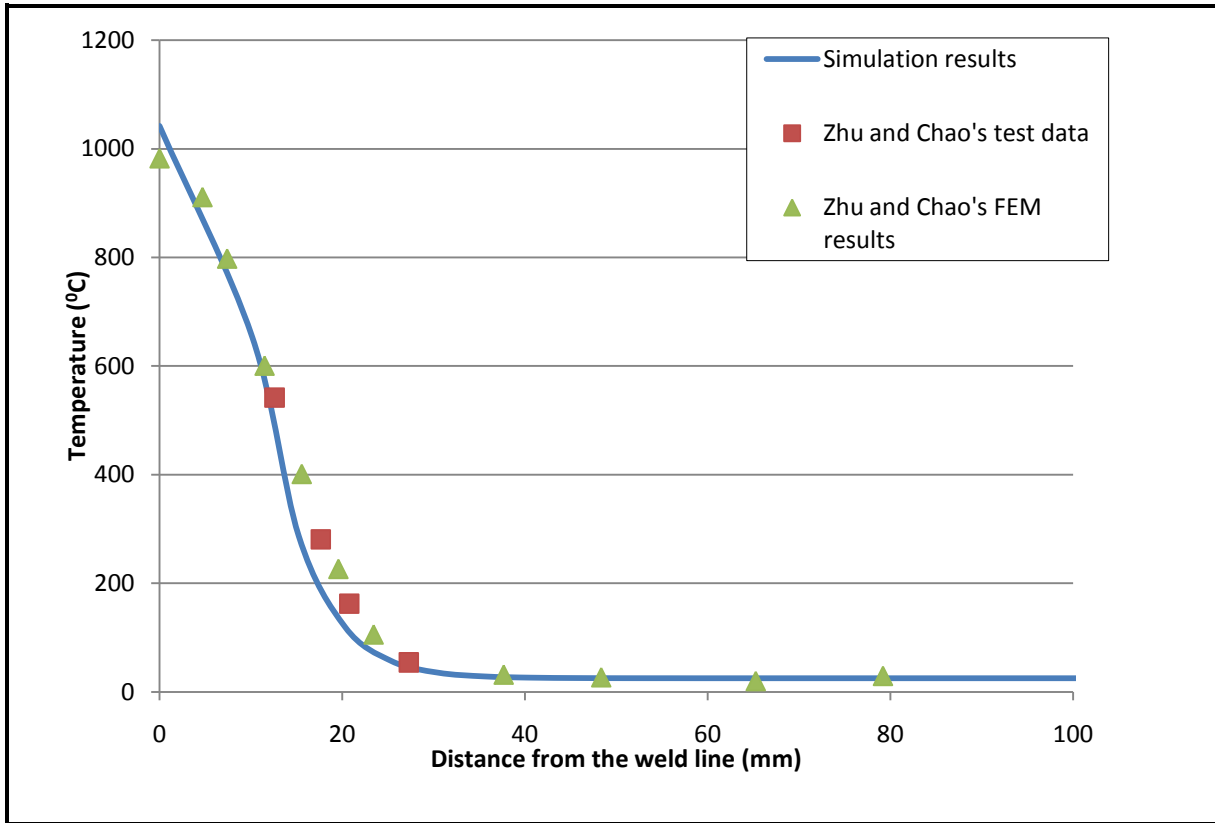


Figure 5.1 Comparison of temperature distribution along the transverse direction at welding time $t=83$ s

Figure 5.2 shows the temperature distribution on the top surface of the workpiece measured at welding time $t=50.4$ sec. Figure 5.3 shows the variation in temperature with respect to time at location $(X=152.4, Y=12.7, Z=0)$ of the workpiece for both the results obtained by Zhu and Chao [28] and by the model developed in this study. The overall trend of the predicted temperature profile is similar to that obtained by Zhu and Chao [28], thus verifying the validity of the model developed in this study.

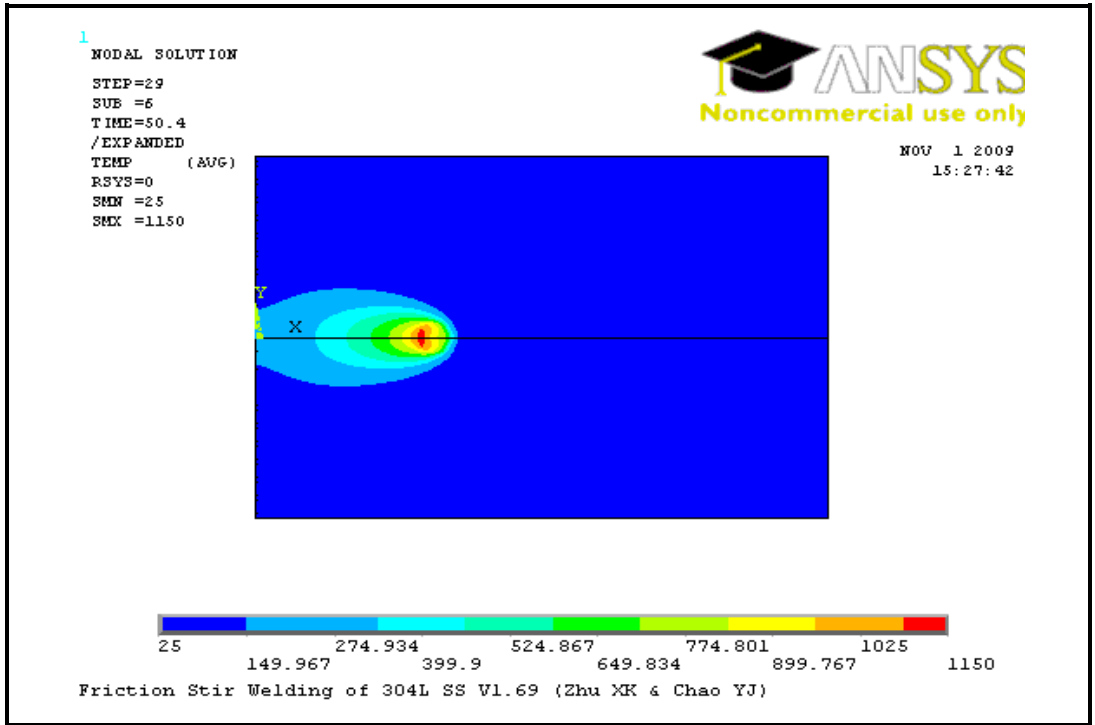


Figure 5.2 Temperature distribution on top surface of the workpiece at welding time, $t= 50.4$ sec

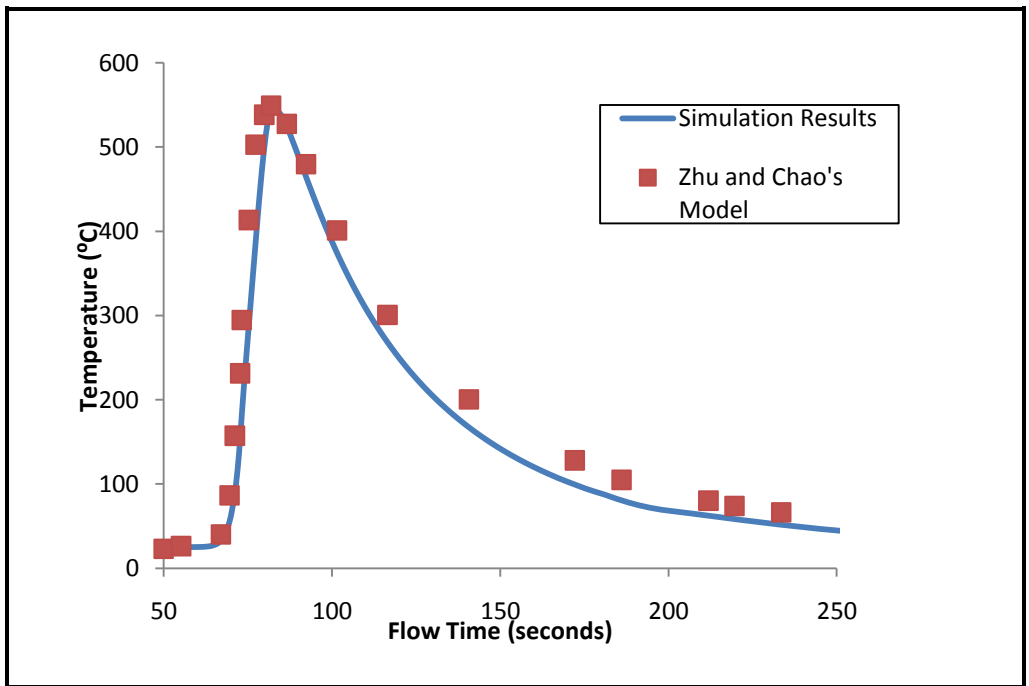


Figure 5.3 Variation of transient temperature - comparison of simulated results and results from Zhu and Chao's Model

5.1.2 Stress Responses

The temperature fields obtained from the thermal model are used as input for the mechanical simulation for calculation of residual stresses. The primary residual stresses in FSW were observed in the longitudinal direction. Therefore, only longitudinal stresses were considered in this study. Figure 5.4 shows the comparison of results from Zhu and Chao's model [28] and simulation results of longitudinal residual stresses for the top surface. The residual stresses were measured along traverse direction at a distance of 152 mm from the end of the workpiece. Fixture release was modeled in order to estimate the effect of clamping. It was observed that the residual stress in the welds decreased significantly after the fixture release. The overall trend of the developed model for prediction of residual stress is similar to that of Zhu and Chao [28], thus verifying the validity of the model developed in this study.

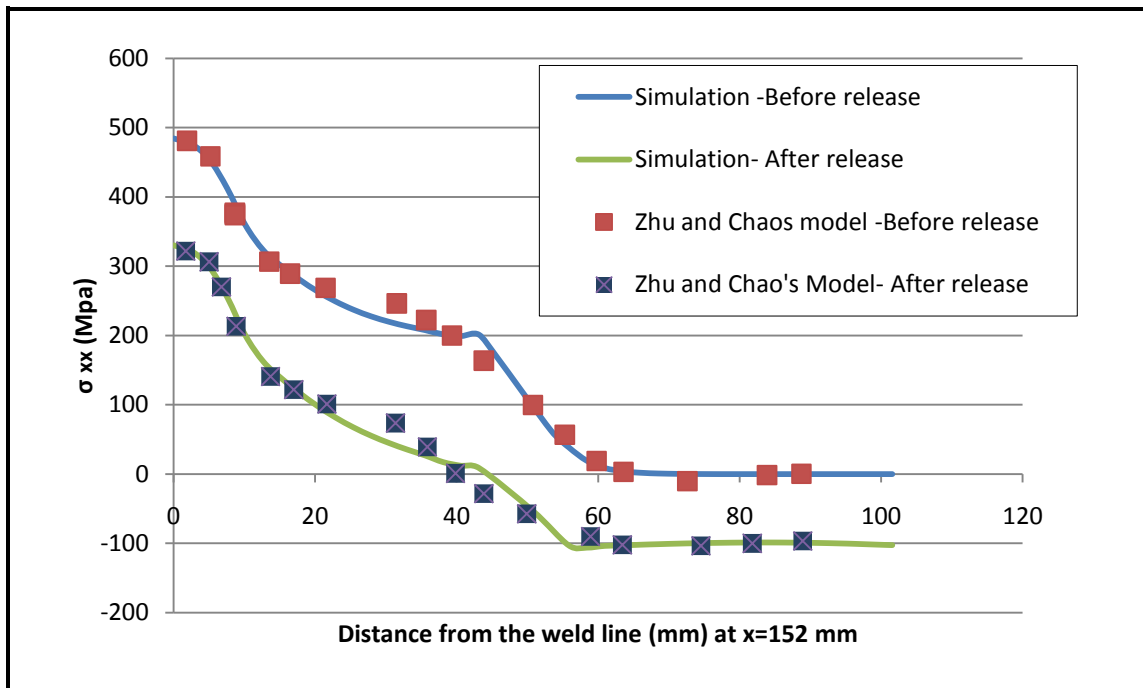


Figure 5.4 Variation of the longitudinal residual stress along the traverse direction at the middle section of the workpiece

6. Parametric Study and Surrogate Models of FSW Process

In order to conduct parametric investigation of FSW process, design of experiment methodology is implemented in this study. Design of experiment (DoE) technique is used to optimize the number of experiments required to determine the effects of various factors affecting the response of the system [56]. DoE helps to eliminate the need for extensive experimental analysis and in turn reduces the computational time and cost. The following sections describe the details of DoE and development of surrogate models for FSW process.

6.1 Design of Experiments

Thermal and thermomechanical models developed in the chapter 4 are used as base models for carrying out parametric studies. An “experiment” in this study would refer to a distinct numerical simulation run for a given set of input parameters. The first step in DoE is to identify important independent input factors and response variables. The response variables selected for this study are maximum temperature (T) and residual stress (R). Both these selected responses are recorded at a selected location i.e. X= 152.4 mm, Y= 0 mm, and Z= 0 mm. The process parameters heat input (H) and welding speed (S) are chosen as input variables affecting the response variable temperature (T), while the parameters H, S and clamping location (C) are chosen variables affecting the response residual stress (R). The next step is to identify the range and the specific levels at which selected factors have to be varied. Table 6.1 lists the process parameters, their range and selected levels used in this study for response variables T and R.

The final step in the parametric design is to perform the required number of experimental runs and analyze the significant factor effects. The total number of experimental runs to be conducted is identified from the total number of factors and the number of levels selected. Table A.1 in appendix A depicts the design matrix for response variable T used in screening design for

parametric study. Table A.2 in appendix A depicts the design matrix for the other selected response, residual stress (R). The observations which exceeded 1450 °C, the melting point of 304L stainless steel, were omitted from design matrix when formulating surrogate models.

Table 6.1 Process parameters, range and design levels used

Response	Process Parameters	Units	Range	Level 1	Level 2	Level 3	Level 4	Level 5
Temperature (T)	Weld Speed (<i>S</i>)	mm/sec	0.5-2.54	0.5	0.85	1.00	1.69	2.54
	Heat Input (<i>H</i>)	watt	500-970	500	600	760	970	-
Residual Stress (R)	Weld Speed (<i>S</i>)	mm/sec	0.5-2.54	0.5	0.85	1.00	1.69	2.54
	Heat Input (<i>H</i>)	watt	500-970	500	600	760	970	-
	Clamping location (<i>C</i>)	mm	50.2-76.2	50.2	76.2	-	-	-

6.1.1 Effect of Factors on Temperature Distribution and Residual Stress

Figures 6.1 and 6.2 depict the plots of main effects for temperature and residual stress, respectively. These plots help to assess the effect of each factor graphically. The figures 6.1 and 6.2 show that heat input factor has a significant effect on both temperature and residual stress and a direct proportionality can be seen between the heat input factor and the responses. Temperature decreases with increasing welding speed. Figure 6.3 shows the variation of temperature on top surface of the workpiece for welding speeds 0.50 mm/s to 2.54 mm/s at constant heat input of 600 W. The peak temperature tends to increase as the welding speed is reduced. On the other hand, it is observed residual stress first increases with increase in welding speed and then tends to slightly decrease at higher welding speeds.

The clamping location also has a significant effect on the residual stress. It is observed from figure 6.2 that if the clamp location is nearer to the weld, lower residual stresses are developed. As the clamp location moves further away from the weld line, level of residual stress increases.

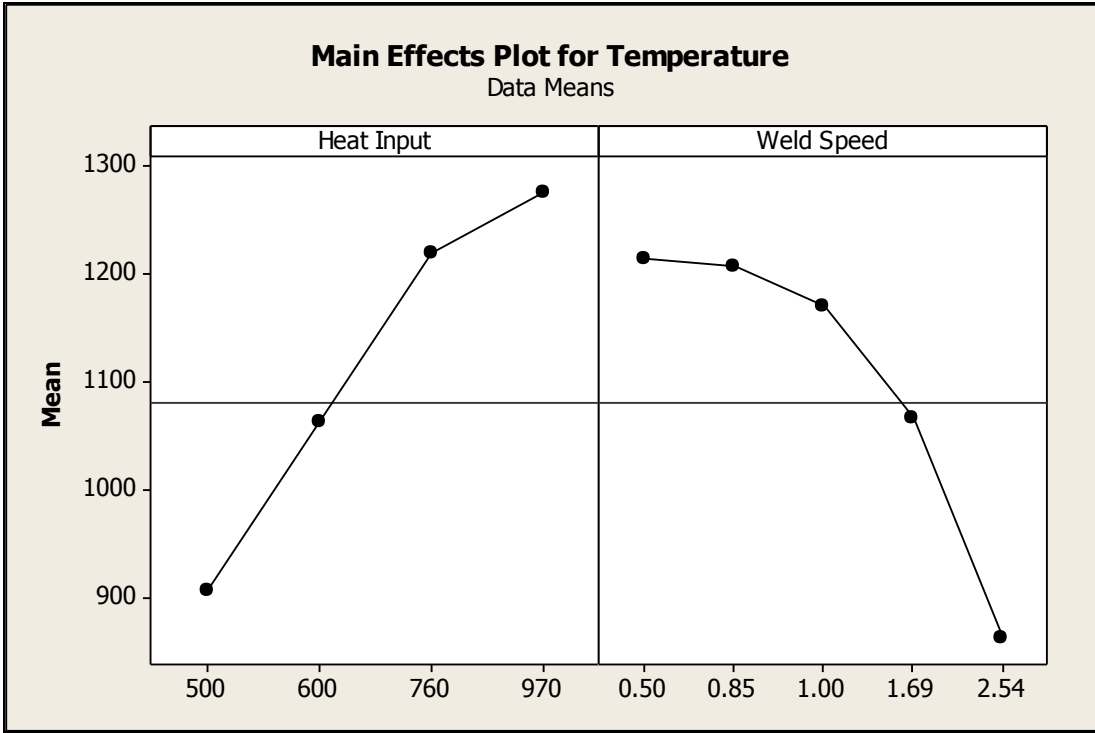


Figure 6.1 Plot of main effects for temperature

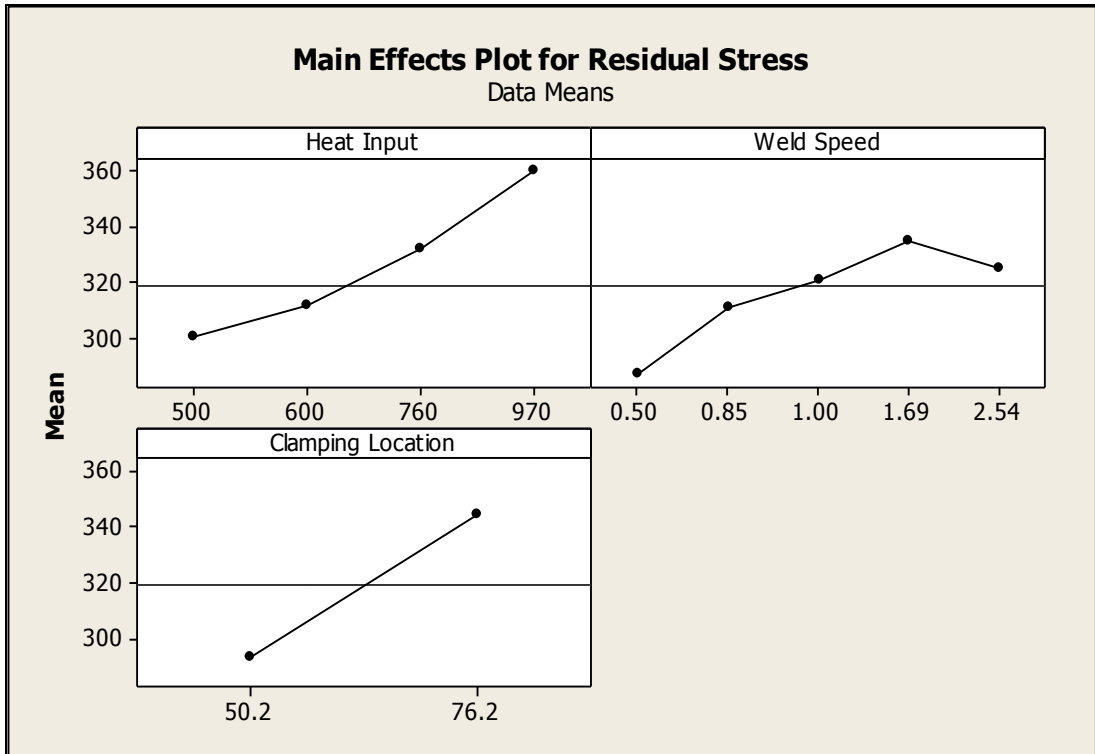


Figure 6.2 Plot of main effects for residual stress

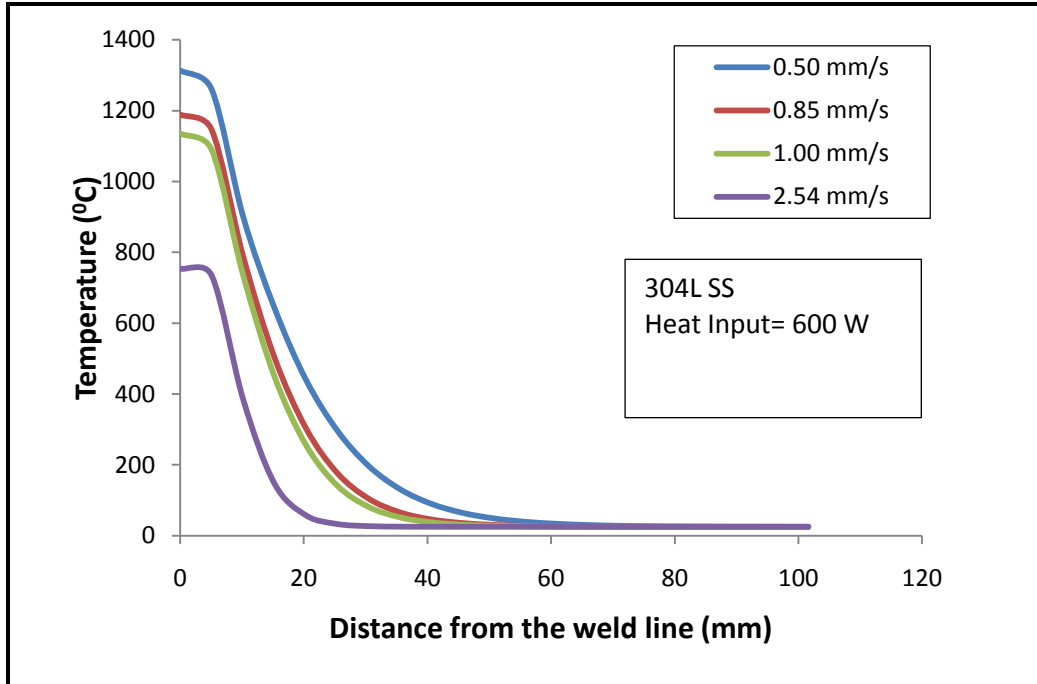


Figure 6.3 Variation of temperature on top surface of the workpiece at different welding speeds

6.2 Surrogate Models of Friction Stir Welding

A surrogate provides fast approximations of the system response and it can be used for optimization studies [57]. A surrogate can be used to model the design objectives or model the constraints. In this study, surrogate models are constructed to establish relationship between the process parameters and the output responses.

A surrogate model for any given set of data can be modeled using linear or nonlinear regression, neural networks, response surface approximations, support vector regression, etc. [47]. In this study, linear and nonlinear regression methods are used to construct surrogate models and later their performances are evaluated.

6.2.1 Development of Model for Response – Temperature

Multiple regression analysis was used to establish relationship between the selected input process parameters and the thermal response variable. Heat input (H) and welding speed (S) are the

selected input process parameters for the response temperature (T). The simulated data obtained in table A.1 in appendix A, is used for setting up surrogate models.

Minitab 15, commercial statistical software capable of data analysis, was used to compute the regression constants for multi-linear regression model. The fitted linear regression model for temperature is given by equation (6.1).

$$T = 647 + 1237 * H - 695 * S \quad (6.1)$$

The results of multiple linear regression analysis are included in appendix B.

Additionally, nonlinear regression models were also setup using the simulated data obtained in table A.1 in appendix A. The nonlinear regression analysis was carried out using DataFit version 9.0, statistical software capable of curve fitting and nonlinear regression analyses. The fitted nonlinear regression model for temperature obtained from DataFit is given by equation (6.2).

$$T = 1844.12 + 881.64 * \ln(H) - 683.56 * S \quad (6.2)$$

The complete nonlinear regression analysis is included in appendix C.

6.2.2 Development of Model for Response – Residual Stress

Multiple regression analysis was used to establish relationship between the selected input process parameters and the thermomechanical response variable. Heat input (H) and welding speed (S) and clamping location (C) are the selected input process parameters for the response residual stress (R). The simulated data obtained in table A.2 in appendix A, is used for setting up surrogate models for residual stress.

The regression constants for multi-linear regression model were calculated using Minitab 15. The fitted linear regression model for residual stress is given by equation (6.3).

$$R = 111 + 115 * H + 12.6 * S + 149 * C \quad (6.3)$$

The results of multiple linear regression analysis are included in appendix B.

Additionally, nonlinear regression model was also setup using the simulated data obtained in table A.2 in appendix A. The nonlinear regression analysis was carried out using DataFit version 9.0. The fitted nonlinear regression model for residual stress obtained from DataFit is given by equation (6.4).

$$R = \exp(0.3486 * H + 0.0417 * S + 0.4689 * C + 5.1119) \quad (6.4)$$

The complete nonlinear regression analysis is included in appendix C.

6.3 Estimation of Performance of Developed Surrogate Models

Two models, one linear and one nonlinear model, were fitted to estimate the temperature of the workpiece at the selected location. Additionally, another two models, one linear and one nonlinear model were fitted to estimate the residual stress at the selected location. The performance and adequacy of the surrogate models was evaluated based on the following statistics:

1. The coefficient of determination (R^2)

R^2 is a statistical measure which indicates how well a regression model describes the given data set. Using this criterion, a model with higher values of R^2 is selected as it indicates a better fit.

2. The residual sum of squares(RSS)

RSS measures the discrepancy between the given dataset and the estimated model. Using this criterion, a model with lower values of residual sum of squares is preferred as it indicates a better fit.

3. The Akaike's information criterion(AIC)

AIC is a parameter independent measure used to compare the relative goodness-of-fit of the predicted models. AIC is estimated by the following equation (6.5).

$$AIC = 2k + n * [\ln(2\pi(RSS)/n) + 1] \quad (6.5)$$

where n is the number of observations, and k is the number of parameters in the model.

The models to be compared are ranked according to their *AIC* and the model with the lowest *AIC* is selected as the best fit model.

4. The adjusted coefficient of determination (R_{adj}^2)

Like *AIC*, the adjusted coefficient of determination is parameter independent and is used as a measure to find the optimal regression model. A higher value of R_{adj}^2 indicates better fit.

The values of R^2 , *RSS*, *AIC* and R_{adj}^2 were used to determine the goodness-of-fit of the surrogate models. Table 6.2 shows the regression statistics of linear and nonlinear surrogate models developed for estimating temperature and residual stress. From table 6.2, it is seen that in case of surrogate models for temperature, the values of R^2 and R_{adj}^2 are higher and the values of *AIC* and *RSS* are lower for nonlinear model when compared to those of linear model. This indicates that the nonlinear model given by equation (6.2) fits the data better than the linear model given by equation (6.1).

Table 6.2 Regression statistics of linear and nonlinear surrogate models

Response Variable	Regression Model	Equation Number	k	R^2	<i>RSS</i>	<i>AIC</i>	R_{adj}^2
Temperature	Linear	(6.1)	3	0.9772	19469	165.07	0.9737
	Nonlinear	(6.2)	3	0.9839	13772	159.53	0.9814
Residual Stress	Linear	(6.3)	4	0.8837	4347	255.98	0.8712
	Nonlinear	(6.4)	4	0.8879	4188	254.78	0.8759

A similar trend was observed for the surrogate models of residual stress. The nonlinear regression model had higher R^2 and R_{adj}^2 values and lower *AIC* and *RSS* values compared to the

linear model, indicating nonlinear linear model given by equation (6.4) has better fit than linear model given by equation (6.3). Thus the best models for estimating the responses, workpiece temperature and residual stress were nonlinear regression models.

7. Determining Optimal FSW Parameters Using Improved Harmony Search Algorithm

The following section describes the model-based approach using Improved Harmony Search (IHS) algorithm applied to the FSW process in this study.

7.1 Formulation of Optimization Problem

The main goal of this research is to develop an optimization strategy to determine process parameters which are able to optimize the weld quality. The search for optimum is based on maximizing the throughput and minimizing the manufacturing costs. Therefore, the optimization problem is formulated as follows [47]:

Maximize Throughput

Minimize Cost

Subject to,

- (i) Maintaining good weld quality
- (ii) The upper and lower limits of the process parameters

The production throughput for a welding process could be measured in terms of the length of weld completed, which in turn relates to the welding speed. Therefore, maximizing the throughput for the process can be interpreted in terms of maximizing the welding speed. The costs relating to welding process include the cost of equipment, labor cost, and cost relating to energy input. However, considering that equipment cost and labor cost are fixed for the process, cost relating to energy input forms the dominant cost component. Further, the weld qualities are the result of thermomechanical history during welding and these weld quality constraints can be equated with constraints on temperature and residual stress. Additional practical constraints are applied from the bounds of process parameter values [47, 54].

In this research, the two conflicting objectives i.e. maximizing speed and minimizing cost are handled by combining them into single objective function with equal weights applied to each of the two objectives. The two objective functions have different units of measurement. To offset the magnitude difference between them, the process variables are normalized by dividing with the maximum value.

The optimization models, formulated based on thermal model, have the following form:

$$\begin{aligned}
 &\mathbf{Minimize} && H - S \\
 &\text{Subjected to: } && T_{LB} \leq T \leq T_{UB} \\
 &&& H_{LB} \leq H \leq H_{UB} \\
 &&& S_{LB} \leq S \leq S_{UB}
 \end{aligned}$$

where, T is the temperature, H is the heat input, and S is the welding speed, LB and UB stands for lower and upper bounds.

Two optimization models are formulated using the surrogate models developed for estimating temperature. These two models differ primarily on the equations for T : called Model 1 if linear equation (6.1) is used, Model 2 if nonlinear equation (6.2) is used instead, for easy reference later.

To avoid optimization solutions that may exceed the desired residual stress limit, the optimization problem is modified by imposing additional constraints on residual stress and clamping location. The optimization models have the following form:

$$\begin{aligned}
 &\mathbf{Minimize} && H - S \\
 &\text{Subjected to: } && T_{LB} \leq T \leq T_{UB}; && H_{LB} \leq H \leq H_{UB} \\
 &&& S_{LB} \leq S \leq S_{UB}; && C_{LB} \leq C \leq C_{UB} \\
 &&& R \leq R_{UB}
 \end{aligned}$$

where C is the location of the clamp from the weld centerline and R is the residual stress.

Two optimization models are formulated based on the above consideration. These two models differ primarily on the equation for T and R : called Model 3 if linear equation (6.1) for T and linear equation (6.3) for R is used, Model 4 if nonlinear equation (6.2) for T and nonlinear equation (6.4) for R is used instead, for easy reference later.

7.2 Solution Methodology Using Harmony Search Algorithm

Metaheuristics are high level heuristic algorithms widely used for solving optimization problems. In general, population-based metaheuristics such as ant colony optimization, genetic algorithm, harmony search, particle swarm optimization etc. are more effective for constrained function optimization problems than single-point search metaheuristics like simulated annealing, tabu search, iterated local search etc. [47]. Harmony Search algorithm (HS), a population-based metaheuristics is selected for this study because the optimization problem formulated for friction stir welding process is a constrained function optimization. HS algorithm is inspired from the musical process of searching for a pleasing harmony and has been successfully applied to various optimization problems [58].

HS algorithm was proposed by Geem et al. [59] in 2001. Unlike ant colony optimization and particle swarm optimization which are inspired from nature/natural phenomenon, harmony search algorithm is inspired from an artificial phenomenon found in musical performance. The process of musicians in a musical performance to produce fantastic harmony pleasing to hear has been compared to the process of optimization in order to find the best solution. The music from combined instruments is judged by aesthetic standards, just as the optimal solution is estimated by objective function. Table 7.1 shows the comparison between optimization process and musical performance.

Table 7.1 Comparison between optimization and musical performance [59]

Comparison Factor	Optimization Process	Performance Process
Best state	Global optimum	Fantastic harmony
Estimated by	Objective function	Aesthetic standard
Estimated with	Values of variables	Pitches of the instruments
Process unit	Each iteration	Each practice

7.2.1 Improved Harmony Search Algorithm

The improved harmony search (IHS) algorithm developed by Mahdavi et al. [60] is implemented for optimization process in this study. An important consideration in the application of optimization methods is how the algorithm handles the constraints relating to the problem [58]. In this study, the constraints are handled using the parameter-less penalty approach proposed by Deb [61]. In Deb's approach, when comparing two solutions, the constraints are handled using the following clauses [61]:

1. When two feasible solutions are compared, the one with better objective value is chosen.
2. When a feasible and an infeasible solution are compared, a feasible solution wins over an infeasible solution.
3. When two infeasible solutions are compared, the one with smaller constraint violation is chosen.

7.2.2 Pseudo Code

The pseudo code of the implemented improved harmony search algorithm, called IHS+, is given below.

Step 1: Initialize the problem and algorithm parameters

The optimization problem is formulated as minimizing the objective function and the

design variable bounds are defined. The algorithm parameters are initialized at this stage. The parameters include the number of solution vectors in the harmony memory i.e. the harmony memory size (HMS), harmony memory considering rate ($HMCR$), maximum and minimum pitch adjusting rate (PAR_{max} , PAR_{min}), maximum and minimum bandwidth (bw_{max} , bw_{min}), and the number of function evaluations or stopping criterion (NI).

Step 2: Initialize the harmony memory

Harmony memory (HM) is initialized with randomly generated harmonies which are within the acceptable design upper and lower bounds [UB , LB]. The infeasible solutions are not eliminated but are handled by using Deb's strategy.

Step 3: Improvise a new harmony

A new harmony vector is generated from HM based on three rules (i) memory consideration, (ii) pitch adjustment and (iii) randomization [62]. The memory consideration ensures that the design variable values are chosen from HS memory while the randomization step ensures random selection of a harmony vector. Pitch adjustment ensures that an adjacent value from initial HM is chosen. This is implemented as follows:

While generation (gn) \leq NI

- a. Update the pitch adjusting rate (PAR) with each generation for fine-tuning of optimized solution vectors, according to equation (6) in Mahdavi et.al. [60], which is denoted by equation (7.1).

$$PAR(gn) = PAR_{min} + \frac{(PAR_{max} - PAR_{min})}{NI} \times gn \quad (7.1)$$

where $PAR(gn)$ is the pitch adjusting rate for each generation

- b. Update the bandwidth (bw) with each generation for fine-tuning of optimized solution vectors, according to equation (7) in Mahdavi et.al. [60], which is denoted by

equation (7.2).

$$bw(gn) = bw_{max} e^{\left(\frac{\ln\left(\frac{bw_{min}}{bw_{max}}\right)}{NI} \times gn \right)} \quad (7.2)$$

where $bw(gn)$ is the bandwidth for each generation.

For each decision variable

- i. Construct a new harmony vector either by choosing each decision variable from any specified HM range based on probability HMCR (memory consideration) or choosing a totally random harmony value from the feasible range with probability of (1-HMCR) (random selection).
- ii. Check if a $rand < PAR$, with $rand$ being a uniformly distributed random value $\in [0, 1]$, and determine whether each component of the new harmony vector obtained from memory consideration should be pitch-adjusted. Construct a new harmony vector by updating the variables which have to be pitch-adjusted by $\pm bw * u(-1,1)$, where $u(-1,1)$ is a uniformly distributed random value between (-1, 1).

End for

Step 4: Update harmony memory

Update the harmony memory by replacing the worst one in the memory with the new one, if the new one improves it. This is handled by ranking the solutions in archive by first giving preference to feasible solutions over infeasible ones, then ranking feasible solutions with respect to their objective values, and finally ranking infeasible solutions in ascending order of constraint violation.

Step 5: Update the best solution and increment gn by one.

End while

Step 6: Output the result of optimal solution and its objective value.

The IHS+ algorithm used in the present study differs from IHS in the following areas. First of all the IHS+ uses Deb's strategy to handle constraints and it allows the use of HM members that violate the constraints. This implementation thus avoids the exhaustive trial and error process of generating a harmony memory with each of its members satisfying all the constraints. Additionally, IHS+ calculates and stores constraint violation information associated with each harmony vector. Further, IHS+ differs from IHS in the way the solutions are ranked and the best solution is selected.

Major parameters associated with the IHS+ algorithm include harmony memory size, HMS , maximum number of function evaluations, NI , harmony memory considering rate, $HMCR$, maximum and minimum pitch adjusting rate, PAR_{max} and PAR_{min} , and maximum and minimum bandwidth, bw_{max} and bw_{min} . The table 7.2 lists the values fixed for the parameters used for this study.

Table 7.2 Parameters used for IHS+ in this study

Parameter	Value	
	Model 1 and Model 2	Model 3 and Model 4
HMS	20	30
NI	100000	150000
$HMCR$	0.9	0.9
PAR_{max}	0.99	0.99
PAR_{min}	0.45	0.45
bw_{max}	4	4
bw_{min}	0.00001	0.00001

7.3 Optimization Results for FSW Process

The IHS+ algorithm was applied to solve the optimization model formulated in the previous section for the targeted friction stir welding process. Due to the stochastic nature of the IHS+ algorithm, for each case, 30 independent runs were made to produce sufficient statistical data. The best, median, and worst results of objective values and CPU time attained in 30 runs were recorded. The solutions for the best results were also recorded. Additionally, for comparison, the optimization problems were solved using the function *fmincon* available in MATLAB Optimization toolbox. The function *fmincon* implements sequential quadratic programming algorithm to find the constraint minimum of a scalar function of several variables starting at an initial estimate [63]. The IHS+ optimization method was implemented in MATLAB. All the programs were run on a 2.66 GHz Intel Pentium-D processor with 2 GB of random access memory.

7.3.1 Results for Model 1 and Model 2

Model 1 uses the fitted linear regression equation of T, i.e. equation (6.1), while the Model 2 uses the fitted nonlinear equation of T, i.e. equation (6.2). These optimization models were solved using a wider bound of T, i.e. $T_{LB} = 1000$ and $T_{UB} = 1300$. The bounds for the other process variables were set at the lowest and highest simulated values, i.e. $H_{LB} = 500$, $H_{UB} = 970$, $S_{LB} = 0.5$ and $S_{UB} = 2.54$. These temperature range and bound values should be set in consideration of material properties and practical experimental constraints. The melting point of 304L stainless steel is about 1450 °C. To enable this study, the bound values selected are a rough guess around known good temperature value below the melting range.

Table 7.3 summarizes the results obtained by IHS+ and *fmincon* function for both the Model 1 and Model 2. The results indicate that:

- (i) The best objective value of -0.152789 with optimal solution $H=821.795$ W and $S=2.54$ mm/s was obtained for Model 1 using both algorithms. While, a lower objective value i.e. -0.166495 and optimal solution $H=808.50$ W and $S=2.54$ mm/s was obtained for Model 2. The result seems to indicate that optimization on Model 2 leads to a better solution.
- (ii) The function *fmincon* found the best solution in all 30 runs. On the other hand, IHS+ algorithm was not able to converge to the best solution in many runs. Nevertheless, the average solution found in all runs is very close to the best.

Table 7.3 Optimization results of Model 1 and Model 2 with $T_{LB} = 1000$ and $T_{UB} = 1300$

		By IHS+		By <i>fmincon</i>	
		Model 1	Model 2	Model 1	Model 2
Objective Value	Best	-0.152789	-0.166495	-0.152789	-0.166495
	Median	-0.152789	-0.166495	-0.152789	-0.166495
	Worst	-0.152789	-0.166494	-0.152789	-0.166495
Best Solution	Heat Input	821.795	808.500	821.795	808.500
	Weld Speed	2.54	2.54	2.54	2.54
CPU Time	Best	16.093750	16.406250	0.015625	0.03125
	Median	16.179688	16.687500	0.03125	0.0625
	Worst	19.484375	16.968750	0.0625	0.093650
Number of runs found the best solution		23	25	30	30

To investigate the effect of narrowing the range of temperature, Model 1 and Model 2 are again solved using a narrower range of T, i.e. $T_{LB} = 1050$ and $T_{UB} = 1150$. Table 7.4 summarizes the results obtained by IHS+ and *fmincon* function for both the Model 1 and Model 2. The results indicate that:

- (i) The best objective value of -0.112369 with optimal solution $H=861.0$ W and $S=2.54$ mm/s was obtained for Model 1 using both algorithms. While, a lower objective value i.e.

-0.117858 and optimal solution $H=855.678$ W and $S=2.54$ mm/s was obtained for Model 2. The result seems to indicate that optimization on Model 2 again leads to a better solution.

(ii) The function *fmincon* found the best solution in all 30 runs. On the other hand, IHS+ algorithm seems not able to converge to the best solution in many runs. Nevertheless, the average solution found in all runs is very close to the best.

(iii) With an increase in lower bound of maximum temperature, T_{LB} , the heat input is forced to increase in order to raise the temperature, which in turn leads to higher objective value.

Table 7.4 Optimization results of Model 1 and Model 2 with $T_{LB} = 1050$ and $T_{UB} = 1150$

		By IHS+		By <i>fmincon</i>	
		Model 1	Model 2	Model 1	Model 2
Objective Value	Best	-0.112369	-0.117858	-0.112369	-0.117858
	Median	-0.112368	-0.117858	-0.112369	-0.117858
	Worst	-0.112368	-0.117858	-0.112369	-0.117858
Best Solution	Heat Input	861.00	855.678	861.00	855.678
	Weld Speed	2.54	2.54	2.54	2.54
CPU Time	Best	16.31250	16.62500	0.03125	0.031250
	Median	16.43750	16.77343	0.03125	0.062500
	Worst	16.90650	17.01562	0.0625	0.093750
Number of runs found the best solution		24	24	30	30

In order to investigate the effect of further narrowing variable bounds, Model 1 and Model 2 are again solved using a tighter range of T, i.e. $T_{LB} = 1140$ and $T_{UB} = 1150$. From optimization point of view, tighter constraints on temperature means increased difficulty in finding optimal solution. Table 7.5 summarizes the results obtained by IHS+ and *fmincon* function for both the Model 1 and Model 2 under tighter constraints. The results indicate that:

- (i) The best objective value of -0.039612 with optimal solution $H=931.576$, W and $S=2.54$ mm/s was obtained for Model 1 using both algorithms. While, a higher objective value i.e. -0.023050 and optimal solution $H=947.64$ W and $S=2.54$ mm/s was obtained for Model 2. This result seems to indicate that optimization on Model 1 leads to a better solution in this particular case.
- (ii) The function *fmincon* found the best solution in all 30 runs. On the other hand, IHS+ algorithm seems not able to converge to the best solution in many runs.
- (iii) With an increase in lower bound of maximum temperature, T_{LB} , the heat input is again forced to increase in order to raise the temperature, which in turn leads to even higher objective values.
- (iv) The corresponding temperature values of all the best solutions in the above cases take on the lower bounds of temperature constraint.

Table 7.5 Optimization results of Model 1 and Model 2 with $T_{LB} = 1140$ and $T_{UB} = 1150$

		By IHS+		By <i>fmincon</i>	
		Model 1	Model 2	Model 1	Model 2
Objective Value	Best	-0.039612	-0.023050	-0.039612	-0.023050
	Median	-0.039612	-0.023050	-0.039612	-0.023050
	Worst	-0.039611	-0.023050	-0.039612	-0.023050
Best Solution	Heat Input	931.57636	947.64053	931.57636	947.6415
	Weld Speed	2.54	2.54	2.54	2.54
CPU Time	Best	16.21875	16.51562	0.015625	0.046875
	Median	16.38281	16.84375	0.031250	0.062500
	Worst	17.01562	17.37500	0.062500	0.109375
Number of runs found the best solution		24	20	30	30

7.3.2 Results for Model 3 and Model 4

In order to find optimal operating process parameters of FSW process which limit the residual stresses, Model 3 and Model 4 are formulated. Model 3 uses the fitted linear regression equation of T, i.e. equation (6.1) and fitted linear regression equation of R, i.e. equation (6.3), while the Model 4 uses the fitted nonlinear equation of T, i.e. equation (6.2) and the fitted nonlinear equation of R, i.e. equation (6.4). The optimization models were constrained by the operating temperature range, maximum residual stress and the bounds of design variables. For this study, the optimization models were solved using a wider bound of T, i.e. $T_{LB}= 1000$ and $T_{UB}= 1300$ and maximum residual stress, R_{UB} , was set at 310. The bounds for the other process variables were set at the lowest and highest simulated values, i.e. $H_{LB}= 500$, $H_{UB}= 970$, $S_{LB}= 0.5$, $S_{UB}= 2.54$, $C_{LB}= 50.2$, and $C_{UB}= 76.2$.

Table 7.6 summarizes the results obtained by IHS+ and *fmincon* function for both the Model 3 and Model 4. The results indicate that:

- (i) The best objective value of -0.100642 with optimal solution $H=756.932$ W, $S=2.238$ mm/s and $C=50.2$ mm was obtained for Model 3 using both algorithms. While, a lower objective value i.e. -0.113535 and optimal solution $H=772.97$ W, $S=2.54$ mm/s and $C=50.2$ mm was obtained for Model 4. This result seems to indicate that optimization on Model 4 leads to a better solution.
- (ii) The function *fmincon* found the best solution in all 30 runs. On the other hand, IHS+ algorithm was not able to converge to the best solution in many runs. Nevertheless, the average solution found in all runs is very close to the best.

To investigate the effect of narrowing the range of temperature, Model 3 and Model 4 are again solved using a narrower range of T, i.e. $T_{LB}= 1050$ and $T_{UB}= 1150$. Table 7.7 summarizes the

results obtained by IHS+ and *fmincon* function for both the Model 3 and Model 4. The results indicate that:

- (i) The best objective value of -0.033843 with optimal solution $H=763.33$ W, $S=2.08$ mm/s and $C=50.2$ mm was obtained for Model 3 using both algorithms. While, a lower objective value i.e. -0.047127 and optimal solution $H=779.85$ W, $S=2.162$ mm/s and $C=50.2$ mm was obtained for Model 4. This result seems to indicate that optimization on Model 4 leads to a better solution.
- (ii) The function *fmincon* found the best solution in all 30 runs. On the other hand, IHS+ algorithm again seems not able to converge to the best solution in many runs. Nevertheless, the average solution found in all runs is very close to the best.
- (iii) With an increase in lower bound of maximum temperature, T_{LB} , the heat input is increased while the velocity is forced to reduce in order to raise the temperature and meet residual stress constraint, which in turn leads to higher objective value.

Table 7.6 Optimization results of Model 3 and Model 4 with constraints $T_{LB} = 1000$, $T_{UB} = 1300$ and $R_{UB} = 310$

		By IHS+		By <i>fmincon</i>	
		Model 3	Model 4	Model 3	Model 4
Objective Value	Best	-0.100642	-0.113535	-0.100642	-0.113535
	Median	-0.100641	-0.113534	-0.100642	-0.113535
	Worst	-0.100639	-0.113533	-0.100642	-0.113535
Best Solution	Heat Input	756.93271	772.970	756.93271	772.970
	Weld Speed	2.238	2.312	2.238	2.312
	Clamping Location	50.20	50.20	50.20	50.20
CPU Time	Best	18.12500	18.109375	0.015625	0.046875
	Median	18.203125	18.632813	0.03125	0.070313
	Worst	19.015625	19.53125	0.109375	1.9375
Number of runs found the best solution		1	13	30	30

Table 7.7 Optimization results of Model 3 and Model 4 with constraints $T_{LB} = 1050$, $T_{UB} = 1150$ and $R_{UB} = 310$

		By IHS+		By <i>fmincon</i>	
		Model 3	Model 4	Model 3	Model 4
Objective Value	Best	-0.033843	-0.047127	-0.033843	-0.047127
	Median	-0.033842	-0.047126	-0.033843	-0.047127
	Worst	-0.033841	-0.047125	-0.033843	-0.047127
Best Solution	Heat Input	763.33083	779.853810	763.33083	779.853810
	Weld Speed	2.08	2.162	2.08	2.162
	Clamping Location	50.20	50.20	50.20	50.20
CPU Time	Best	18.140625	18.156250	0.03125	0.031250
	Median	18.40625	18.632813	0.03125	0.062500
	Worst	19.671875	19.843750	0.0625	0.125000
Number of runs found the best solution		11	6	30	30

8. Validation of Optimization Results

In order to validate the optimization results, finite element analysis (FEA) simulations were carried out according to the process parameters that were obtained from the optimization scheme. Table 8.1 presents the summary of optimal results obtained for different cases for response variable, temperature. The results indicate that the developed models were able to predict the temperature with a reasonable accuracy.

Table 8.1 Summary of results for response - temperature

		Temperature Constraint Range		
		1000-1300	1050-1150	1140-1150
Optimal Solution	Heat Input (W)	808.50	855.678	931.576
	Weld Speed (mm/s)	2.54	2.54	2.54
Model	Best Model	Model 2	Model 2	Model 1
	Regression Type	Nonlinear	Nonlinear	Linear
Output Temperature (°C)	Model Predicted	999.9998	1050.001	1140.0
	FEA Simulation	977.678	1029.43	1112.8
	Error %	2.2831	1.9982	2.4442

The figure 8.1 shows the temperature contour at the selected location i.e. $X=152.4$, $Y=0$, and $Z=0$ for the optimal parameters corresponding to temperature constraint range 1000-1300°C. The peak temperature obtained with optimal parameters as $H= 808.5$ W and $S= 2.54$ mm/s is 977.67°C, while that predicted by the best model is 999.99°C. The Model 2 in this case overestimated the temperature by about 2.28%. From table 8.1, it is seen that the corresponding temperature values of all the optimal solutions take on the lower bounds of temperature constraint.

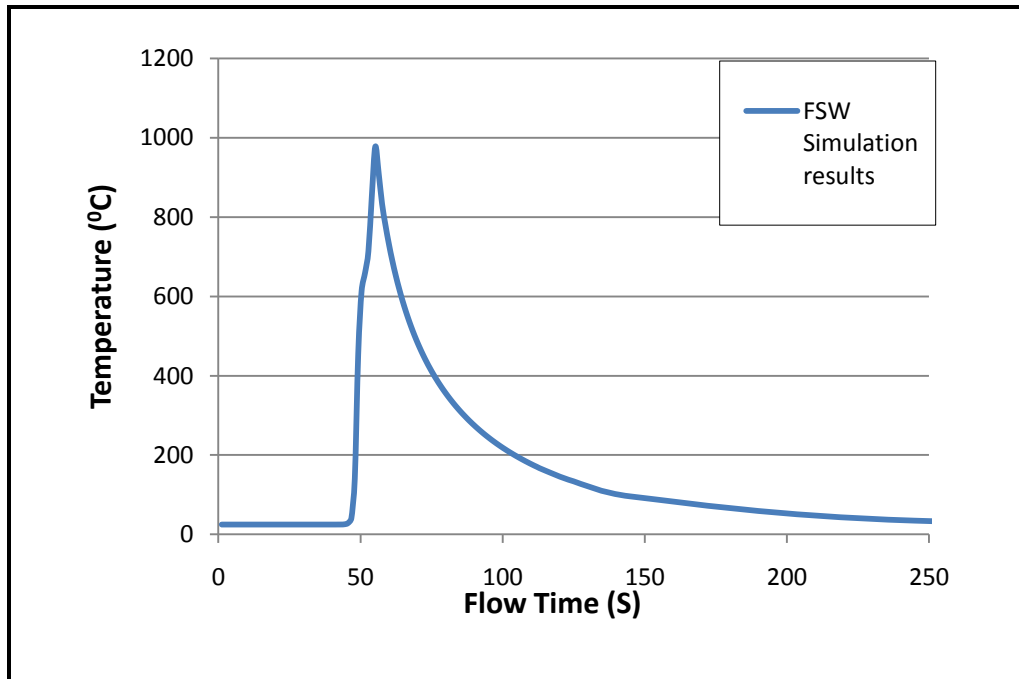


Figure 8.1 Temperature profile at X=152.4, Y=0, Z=0 for optimal parameters H= 808.5 W and S= 2.54 mm/s

Model 3 and Model 4 have additional constraints on the maximum level of residual stresses that can be reached. Table 8.2 presents the summary of optimal results obtained for different cases for the two response variables, temperature and residual stress.

Table 8.2 Summary of results for responses - temperature and residual stress

		Temperature Constraint Range		
		1000-1300	1050-1150	
Optimal Solution		Heat Input(W)	772.970	779.8538
		Weld Speed(mm/s)	2.312	2.162
		Clamping Location (mm)	50.2	50.2
Model		Best Model	Model 4	Model 4
		Regression Type	Nonlinear	Nonlinear
Output	Temperature (°C)	Model Predicted	1021.618	1069.978
		FEA Simulation	991.216	1036.87
		Error %	3.0671	3.1930
	Residual Stress (MPa)	Model Predicted	309.9971	309.9973
		FEA Simulation	316.597	323.247

		Error %	-2.0846	-4.0989
--	--	---------	---------	---------

In order to validate the results for the optimization Model 4, thermomechanical simulations were carried out. The figure 8.2 shows the temperature profile at the selected location i.e. $X=152.4$, $Y=0$, and $Z=0$ for the optimal parameters corresponding to temperature constraint range 1000 - 1300°C. The peak temperature obtained with optimal parameters as $H= 772.97$ W, $S= 2.312$ mm/s and $C=50.2$ mm is about 991.216°C, while that predicted by the best model is 1021.618 °C.

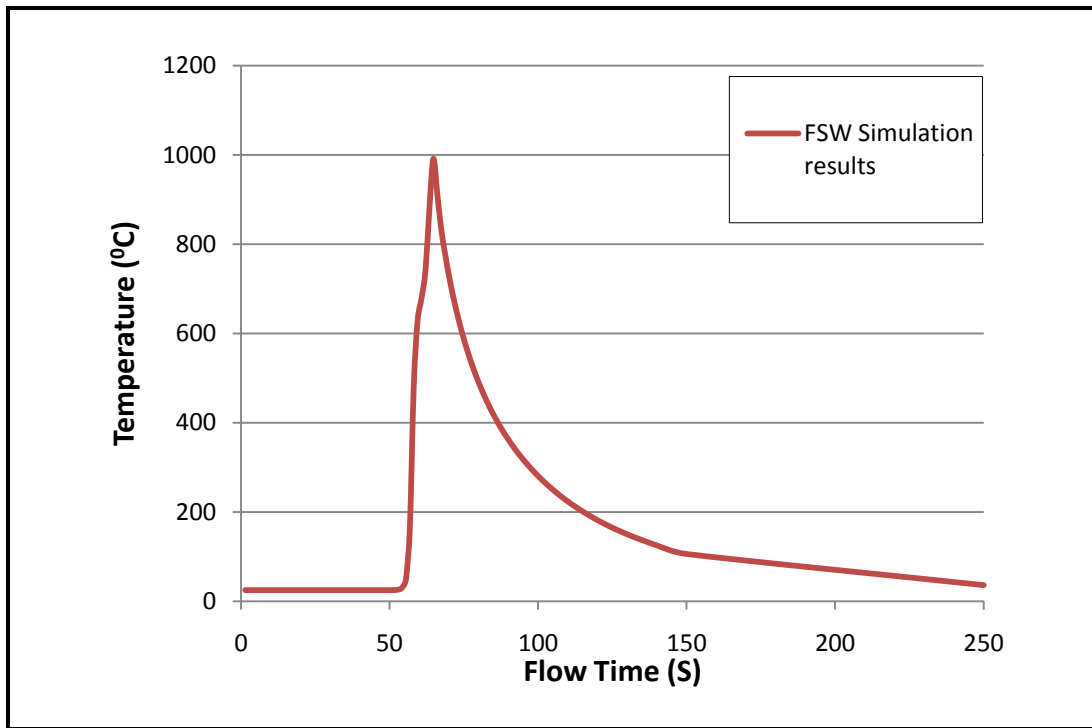


Figure 8.2 Temperature profile at $X=152.4$, $Y=0$ m $Z=0$ for optimal parameters $H= 772.97$ W and $S= 2.312$ mm/s

The corresponding longitudinal residual stress developed during the process operating at the optimal parameters $H= 772.97$ W, $S= 2.312$ mm/s and $C= 50.2$ mm are shown in figure 8.3. The residual stresses on top surface are plotted at distance a distance of $x =152.4$ mm along the traverse direction. The residual stress obtained from FEA at the selected location $X=152.4$, $Y=0$, and $Z=0$ is about 316.597 MPa, while that predicted by the Model 4 is 309.997 MPa. It was observed that the clamping constraints had some localized effect on the stress components in the

unaffected parent material [30]. Both the temperature and residual stress constraints are satisfied by the Model 4. The error in predicting the temperature is about 3.06%, while the error in predicting residual stress is about - 2.08%.

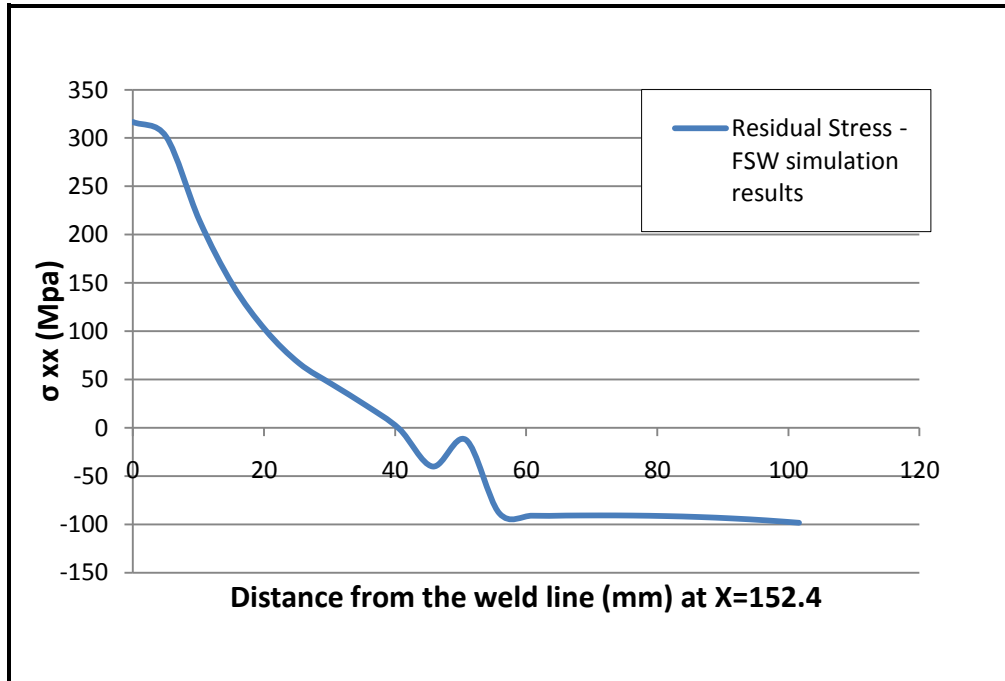


Figure 8.3 Variation of the longitudinal residual stress along traverse direction operating at optimal parameters $H= 772.97$ W, $S= 2.312$ mm/s and $C= 50.2$ mm

9. Conclusions and Recommendations for Future Work

In this research a thermomechanical model of friction stir welding process was reproduced and a surrogate model-based optimization scheme was implemented to obtain the optimal parameters for the process. The thermomechanical model selected for implementation was developed by Zhu and Chao [28] for friction stir welding of 304L stainless steel. The selected finite element model was replicated using ANSYS[®] and validated with the published results. The validated model was then used to simulate the process. A design of experiments and parametric study were performed to identify the effect of various input parameters like: heat input, welding speed and clamping location on temperature distribution and residual stress in the workpiece. Later, linear and nonlinear surrogate models were developed using regression analysis to relate the selected process input parameters with the response variables. Finally, constrained optimization models were formulated using surrogate models with the goal of maximizing throughput and minimizing cost under constraints of achieving desired weld quality and satisfying the operating constraints. The optimization problems were solved using the improved harmony search algorithm [60], enhanced with the parameter-less penalty method proposed by Deb [61] to handle the constraints.

Based on the models developed, the parametric studies and the optimization results, the following observations were made:

1. From the parametric study, it was observed that the workpiece temperature decreases as the welding speed increases, while the residual stress first increases with increase in welding speed and then tends to slightly decrease at higher welding speeds.
2. Clamping location has significant effect on the level of residual stress developed. It was observed that clamping workpiece far from the weld resulted in higher residual stresses.

3. When solving all the optimization models, it was observed that IHS+ was not able to converge to the best solution in many runs. Nevertheless, the average solution found in all runs was very close to the best. Further, from practical point of view this deviation from optimal might be relatively less than accuracy of the physical system and hence might be insignificant in practice.
4. Optimization models formulated in this study were solved easily by *fmincon* function utilizing gradient based technique. However, IHS+ could be useful to solve more complicated problems involving discrete variables where conventional gradient based techniques cannot be applied.
5. The optimum parameters for FSW process were obtained and summarized in tables 8.1 and 8.2. These optimal solutions were verified by the results obtained from finite element analysis.
6. Optimization on Model 2, i.e. nonlinear surrogate model, produced better results when wide temperature range was used. However, for tight temperature constraints, optimization on Model 1, i.e. linear surrogate model, produced better results.
7. Optimization results show that in order to minimize the objective value, welding speed must be maintained at its maximum value while keeping heat input as low as possible. In case of Model 1 and Model 2, when the lower bound of maximum temperature is raised, the heat input is forced to increase in order to raise the temperature. This leads to higher objective values.
8. In case of Model 3 and Model 4, it was observed that to satisfy additional residual stress constraints, the heat input had to be increased while the welding speed had to be reduced to satisfy all the constraints.

For future work, experimental investigations need to be carried out to verify the numerical simulations and optimal solutions obtained in this thesis. The process variables used in this study were limited to responses, maximum temperature and residual stress and the following input variables: heat input, weld speed, and clamping location. The optimization can be performed on a process model that includes more input process variables and output responses. The materials to be welded are considered identical in this study. Similar studies can be extended to other variants of friction stir welding processes such as laser-assisted friction stir welding process, or the welding of dissimilar materials that will be technically more challenging due to the differences in material properties. More comprehensive thermal-material-mechanical models could also be considered for optimization.

References

1. Thomas, W.M., Nicholas, E.D., Needham, J.C., Murch, M.G., Temple-Smith, P., and Dawes, C.J., *Friction-stir butt welding*, GB Patent No. 9125978.8, International patent application No. PCT/GB92/02203, (1991).
2. Thomas, W.M., Threadgill P.L., and Nicholas, E.D., *Friction stir welding of steel: Part one*, <http://steel.keytometals.com/default.aspx?ID=CheckArticle&NM=219>.
3. Nandan, R., DebRoy, T., and Bhadeshia, H., *Recent advances in friction-stir welding - Process, weldment structure and properties*. Progress in Materials Science, 2008. **53**(6): p. 980-1023.
4. Friction Stir Link Inc, <http://www.frictionstirlink.com/fslfswdescription.html>.
5. Lienert, T.J., Stellwag, W.L., Grimmitt, B.B., and Warke, R.W., *Friction stir welding studies on mild steel - Process results, microstructures, and mechanical properties are reported*. Welding Journal, 2003. **82**(1): p. 1S-9S.
6. Zettler, R., Donath, T., dos Santos, J.F., Beckman, F., and Lohwasser, D., *Validation of marker material flow in 4mm thick frictionstir welded Al2024-T351 through computer microtomography and dedicated metallographic techniques*. Advanced Engineering Materials, 2006. **8**(6): p. 487-490.
7. Sorensen, C.D. and Nelson T.W., *Friction Stir Welding of Ferrous and Nickel Alloys*, in *Friction stir welding and processing*, Mahoney, M. W. and Mishra, R.S., Editors. 2007, ASM International: Materials Park, Ohio. p. 111-121.
8. Park, S.H.C., Sato, Y.S., Kokawa, H., Okamoto, K., Hirano, S., and Inagaki, M., *Microstructural characterization of stir zone containing residual ferrite in friction stir welded 304 austenitic stainless steel*. Science and Technology of Welding and Joining, 2005. **10**(5): p. 550-556.
9. Park, S.H.C., Sato, Y.S., Kokawa, H., Okamoto, K., Hirano, S., and Inagaki, M., *Rapid formation of the sigma phase in 304 stainless steel during friction stir welding*. Scripta Materialia, 2003. **49**(12): p. 1175-1180.
10. Ozekcin, A., Jin, H.W., Koo, J.Y., Bangaru, N.V., Ayer, R., Vaughn, G., Steel, R., and Packer, S., *A microstructural study of friction stir welded joints of carbon steels*. International Journal of Offshore and Polar Engineering, 2004. **14**(4): p.284-288.
11. Reynolds, A.P., Tang, W., Gnaupel-herold, T., and Prask, H., *Structure, properties, and residual stress of 304L stainless steel friction stir welds*. Scripta Materialia, 2003. **48**(9): p. 1289-1294.
12. Posada, M., Nguyen, J.P., Forrest, D.R., DeLoach J.J., and DeNale, R., *Friction stir welding advances joining technology*, The AMPTIAC Quarterly, 2003. **7**(3): p.13-20.

13. Threadgill P.L., and Johnson R., *The potential for friction stir welding in oil and gas applications*. Proceedings of the Fourth International Offshore and Polar Engineering Conference, France, ISOPE, 2004. p.1-7.
14. Defalco, J., and Steel, R., *Friction stir process now welds steel pipe*, Welding Journal, 2009. **88**(5): p.44-48.
15. Bhat, B.N., Carter, R.W., Ding, R.J., Lawless, K.G., Nunes, A.V., Russell, C.K., and Shah, S.R., *Friction stir welding development at NASA- Marshall Space Flight Center*, Friction Stir Welding and Processing, Jata, K.V., et al., Editor. 2001, TMS. P. 117-128.
16. Benyounis, K.Y. and Olabi, A.G., *Optimization of different welding processes using statistical and numerical approaches - A reference guide*. Advances in Engineering Software, 2008. **39**(6): p. 483-496.
17. Feng, Z., *Processes and mechanisms of welding residual stress and distortion*. Woodhead Publishing in materials. 2005, Boca Raton, Fla.: CRC Press.
18. TWI, <http://www.twi.co.uk/content/ksrhl001.html>.
19. Kudryavtsev, Y.F., *Residual stress*, in *Springer handbook of experimental solid mechanics*, Sharpe, W.N., Editor. 2008, New York: Springer. p. 371-388.
20. Gould, J.E. and Feng Z.L., *Heat flow model for friction stir welding of aluminum alloys* Journal of Materials Processing & Manufacturing Science, 1999. **7**(2): p. 185-194.
21. Chao, Y.J., Qi, X., and Tang, W., *Heat transfer in friction stir welding - Experimental and numerical studies*, Journal of Manufacturing Science and Engineering-Transactions of the ASME, 2003. **125**(1): p. 138-145.
22. Colegrove P, *3 Dimensional flow and thermal modeling of the Friction Stir Welding process*, in: the Second FSW Symposium, Gothenburg, Sweden, 2000.
23. Khandkar, M.Z.H., Khan, J.A., and Reynolds A.P., *Prediction of temperature distribution and thermal history during friction stir welding: input torque based model*, Science and Technology of Welding and Joining, 2003. **8**(3): p. 165-174.
24. Song, M. and Kovacevic, R., *Heat transfer modelling for both workpiece and tool in the friction stir welding process: a coupled model*. Proceedings of the Institution of Mechanical Engineers Part B-Journal of Engineering Manufacture, 2004. **218**(1): p. 17-33.
25. Vilaca, P., Quintino, L., and dos Santos, J.F., *iSTIR - Analytical thermal model for friction stir welding*. Journal of Materials Processing Technology, 2005. **169**(3): p. 452-465.
26. Chao, Y.J. and Qi, X.H., *Thermal and thermo-mechanical modeling of friction stir welding of aluminum alloy 6061-T6*. Journal of Materials Processing & Manufacturing Science, 1998. **7**(2): p. 215-233.

27. Chen, C.M. and Kovacevic, R., *Finite element modeling of friction stir welding - thermal and thermomechanical analysis*. International Journal of Machine Tools & Manufacture, 2003. **43**(13): p. 1319-1326
28. Zhu, X.K. and Chao, Y.J., *Numerical simulation of transient temperature and residual stresses in friction stir welding of 304L stainless steel*, Journal of Materials Processing Technology, 2004. **146**(2): p. 263-272.
29. Soundararajan, V., Zekovic, S., and Kovacevic, R., *Thermo-mechanical model with adaptive boundary conditions for friction stir welding of Al 6061*. International Journal of Machine Tools & Manufacture, 2005. **45**(14): p. 1577-1587.
30. Khandkar, M.Z.H., Khan, J.A., Reynolds, A.P., and Sutton, M.A., *Predicting residual thermal stresses in friction stir welded metals*. Journal of Materials Processing Technology, 2006. **174**(1-3): p. 195-203.
31. Feng, Z., Wang, X.L., David, S.A., and Sklad, P.S., *Modelling of residual stresses and property distributions in friction stir welds of aluminum alloy 6061-T6*. Science and Technology of Welding and Joining, 2007. **12**(4): p. 348-356
32. Li, T., Shi, Q.Y., and Li, H.K., *Residual stresses simulation for friction stir welded joint*. Science and Technology of Welding and Joining, 2007. **12**(8): p. 664-670.
33. Bastier, A., Maitournam, M.H., Roger, F., and Van, K.D., *Modelling of the residual state of friction stir welded plates*. Journal of Materials Processing Technology, 2008. **200**(1-3): p. 25-37.
34. Peel, M., Steuwer, A., Preuss, M., and Withers, P.J., *Microstructure, mechanical properties and residual stresses as a function of welding speed in aluminum AA5083 friction stir welds*. Acta Materialia, 2003. **51**(16): p. 4791-4801.
35. Staron, P., Kocak, M., Williams, S., and Wescott, A., *Residual stress in friction stir-welded Al sheets*. Physica B: Condensed Matter, 2004. **350**(1-3, Supplement 1): p. E491-E493.
36. Dattoma, V., De Giorgi, M., and Nobile, R., *On the Residual Stress Field in the Aluminium Alloy FSW Joints*. Strain, 2009. **45**(4): p. 380-386.
37. Squillace, A., Segreto, T., Prisco, U., Teti, R., and Campanile G., *Optimization of friction stir welds of aluminum alloys*. Second IPROMS NoE Virtual International Conference on Intelligent Production Machines and Systems, 2006.
38. Meng, Z., Chen, H., and Yue, X., *International Federation for Information Processing (IFIP)*, in Knowledge Enterprise: Intelligent Strategies In Product Design, Manufacturing, and Management. Wang K., et al. Editors. 2006, Springer. p. 483-491.
39. Fratini, L. and Corona, V., *Friction stir welding lap joint resistance optimization through gradient techniques*. Journal of Manufacturing Science and Engineering-Transactions of the Asme, 2007. **129**(6): p. 985-990.

40. Nandan, R., Lienert, T.J., and DebRoy, T., *Toward reliable calculations of heat and plastic flow during friction stir welding of Ti-6Al-4V alloy*. International Journal of Materials Research, 2008. **99**(4): p. 434-444.
41. Okuyucu, H., Kurt, A., and Arcaklioglu, E., *Artificial neural network application to the friction-stir welding of aluminum plates*. Materials & Design, 2007. **28**(1): p. 78-84.
42. Lakshminarayanan, A.K. and Balasubramanian, V., *Process parameters optimization for friction stir welding of RDE-40 aluminium alloy using Taguchi technique*. Transactions of Nonferrous Metals Society of China, 2008. **18**(3): p. 548-554.
43. Jayaraman, M., Sivasubramanian, R., Balasubramanian, V., and Lakshminarayanan, A.K., *Optimization of process parameters for friction stir welding of cast aluminium alloy A319 by Taguchi method*. Journal of Scientific & Industrial Research, 2009. **68**(1): p. 36-43.
44. Larsen, A.A., *Process Optimization of Friction Stir Welding Based on Thermal Models*, in *Department of Mathematics* 2009, Technical University of Denmark. p. 1-110.
45. Elangovan, K., Balasubramanian, V., and Babu, S., *Predicting tensile strength of friction stir welded AA6061 aluminium alloy joints by a mathematical model*. Material & Design, 2009. **30**(1): p.188-193.
46. Babu S., Elangovan K., Balasubramanian V., and Balasubramanian, M., *Optimizing friction stir welding parameters to maximize tensile strength of AA2219 Aluminium alloy joints*. Metals and Materials International, 2009. **15**(2): p. 321-330.
47. Liao, T.W. and Daftardar, S., *Model based optimization of friction stir welding processes*. Science and Technology of Welding & Joining, 2009. **14**(10): p.426-435.
48. Huebner, H.H., Dewhurst, D.L., Smith, D. E., and Byrom, T. G. *The finite element method for engineers*. 4th ed. 2001, New York: J. Wiley.
49. ANSYS[®] *Release 11.0 Documentation*, ANSYS Inc, 2008.
50. Rajdaj, D., *Heat effects of welding: temperature field, residual stress, distortion*. 1992, Berlin, New York: Springer.
51. Kim, Y.C., Fuji, A., and North T.H., *Residual –Stress and Plastic Strain in AISI 304L Stainless Steel Titanium Friction Welds*. Materials Science and Technology, 1995. **11**(4): p. 383-388.
52. Nandan, R., Roy, G.G., Lienert, T.J., and DebRoy, T., *Numerical modelling of 3D plastic flow and heat transfer during friction stir welding of stainless steel*. Science and Technology of Welding and Joining, 2006. **11**(5): p. 526-537.
53. Naidu, R. *Friction Stir Welding: Thermal Effects of a Parametric Study on Butt and Lap Welds*, MS Thesis, Wichita State University, 2006.

54. Daftardar, S., *Laser Assisted Friction Stir Welding: Finite Volume Method and Metaheuristic Optimization*, MS Thesis, Louisiana State University, 2009.
55. Stephens, R.I., Fatemi, A., Stephens, R.R., and Fuchs, H.O., *Metal fatigue in engineering*. 2001, New York: Wiley.
56. Dasgupta, A., Pecht, M.G., and Mathieu, B., *Design-of-experiment methods for computational parametric studies in electronic packaging*. Finite Elements in Analysis and Design, 1998. **30**(1-2): p. 125-146.
57. Mack, Y., Goel, T., Shyy, W., and Haftka, R., *Surrogate Model-Based Optimization Framework: A Case Study in Aerospace Design*. 2007. p. 323-342.
58. Coelho, L.D. and Mariani, V.C., *An improved harmony search algorithm for power economic load dispatch*. Energy Conversion and Management, 2009. **50**(10): p. 2522-2526.
59. Geem, Z.W., Kim, J.H., and Loganathan, G.V., *A new heuristic optimization algorithm: Harmony search*. Simulation, 2001. **76**(2): p. 60-68.
60. Mahdavi, M., Fesanghary, M., and Damangir, E., *An improved harmony search algorithm for solving optimization problems*. Applied Mathematics and Computation, 2007. **188**(2): p. 1567-1579.
61. Deb, K., *An efficient constraint handling method for genetic algorithms*. Computer Methods in Applied Mechanics and Engineering, 2000. **186**: p. 311-338.
62. Lee, K.S. and Geem, Z.W., *A new meta-heuristic algorithm for continuous engineering optimization: harmony search theory and practice*. Computer Methods in Applied Mechanics and Engineering, 2005. **194**(36-38): p. 3902-3933.
63. MATLAB, *Optimization Toolbox–User’s Guide Version 4*, Mathworks Inc., Massachusetts, 2009.

Appendix A: Summary of Simulated Data

Table A.1 Design matrix with factors, selected levels and recorded response temperature (T) for parametric study

Heat Input (watt) <i>H</i>	Weld Speed (mm/s) <i>S</i>	Temperature (°C) <i>T</i>
500	0.50	1117.721
500	0.85	1012.28
500	1.00	967.505
500	1.69	795.271
500	2.54	643.857
600	0.50	1313.42
600	0.85	1188.72
600	1.00	1135.30
600	1.69	928.272
600	2.54	753.712
760	0.50	>1450
760	0.85	1424.85
760	1.00	1407.68
760	1.69	1146.799
760	2.54	903.794
970	0.50	>1450
970	0.85	>1450
970	1.00	>1450
970	1.69	1396.29
970	2.54	1155.04

Table A.2 Design matrix with factors, selected levels and recorded response residual stress (R) for parametric study

Heat Input (watt) <i>H</i>	Weld Speed (mm/s) <i>S</i>	Clamping location (mm) <i>C</i>	Residual Stress (MPa) <i>R</i>
500	0.50	50.2	267.36
500	0.50	76.2	293.34
500	0.85	50.2	282.85
500	0.85	76.2	329.84
500	1.00	50.2	288.48
500	1.00	76.2	341.73
500	1.69	50.2	277.23
500	1.69	76.2	332.59
500	2.54	50.2	262.07
500	2.54	76.2	326.83
600	0.50	50.2	282.93
600	0.50	76.2	305.37
600	0.85	50.2	286.44
600	0.85	76.2	332.33
600	1.00	50.2	293.76
600	1.00	76.2	346.61
600	1.69	50.2	300.69
600	1.69	76.2	355.41
600	2.54	50.2	277.70
600	2.54	76.2	335.49
760	0.85	50.2	292.53
760	0.85	76.2	342.09
760	1.00	50.2	297.64
760	1.00	76.2	354.28
760	1.69	50.2	317.78
760	1.69	76.2	374.83
760	2.54	50.2	309.39
760	2.54	76.2	363.14
970	1.69	50.2	329.09
970	1.69	76.2	389.26
970	2.54	50.2	332.43
970	2.54	76.2	388.92

Appendix B: Multiple Linear Regression Analysis

B.1 Regression Model for Response Temperature Using Minitab 15

The regression equation is: $T = 647 + 1237 * H - 695 * S$

Table B.1 Regression variable results

Predictor	Coef	Standard Error	t-ratio	Prob(t)
Constant	1646.59	42.82	15.10	0.0
Heat Input	1236.81	64.68	19.12	0.0
Weld Speed	-694.52	35.77	-19.42	0.0

Table B.2 Linear regression summary statistics

Standard Error of the Estimate	38.6989
Coefficient of Multiple Determination (R^2)	0.9772
Adjusted Coefficient of Multiple Determination (R^2_{adj})	0.9737
Durbin-Watson Statistic	0.9207

Table B.3 Variance Analysis (ANOVA)

Source	DF	Sum of Squares	Mean Square	F Ratio	Prob(F)
Regression	2	836805	418402	279.38	0.0
Error	13	19469	1498		
Total	15	856273			

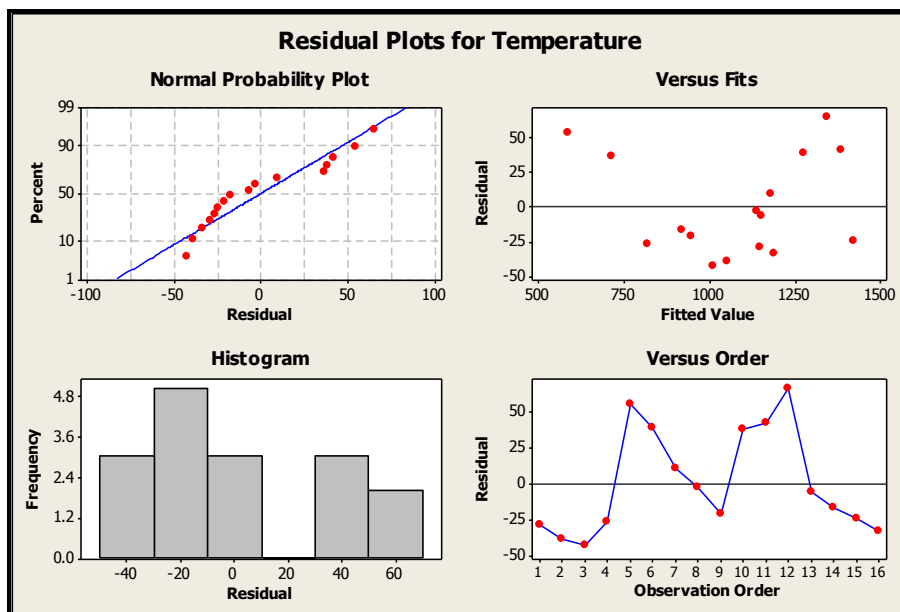


Figure B.1 Residual plots for response Temperature

B.2 Regression Model for Response Residual Stress Using Minitab 15

The regression equation is: $R = 111 + 115 * H + 12.6 * S + 149 * C$

Table B.4 Regression variable results

Predictor	Coef	Standard Error	t-ratio	Prob(t)
Constant	110.76	14.48	7.65	0.0
Heat Input	114.63	14.73	7.78	0.0
Weld Speed	12.625	8.143	1.55	0.132
Clamping Location	149.05	12.91	11.54	0.0

Table B.5 Linear regression summary statistics

Standard Error of the Estimate	12.4601
Coefficient of Multiple Determination (R^2)	0.8837
Adjusted Coefficient of Multiple Determination (R^2_{adj})	0.8712
Durbin-Watson Statistic	1.6627

Table B.6 Variance Analysis (ANOVA)

Source	DF	Sum of Squares	Mean Square	F Ratio	Prob(F)
Regression	3	33046	11015	70.95	0.0
Error	28	4347	155		
Total	31	37393			

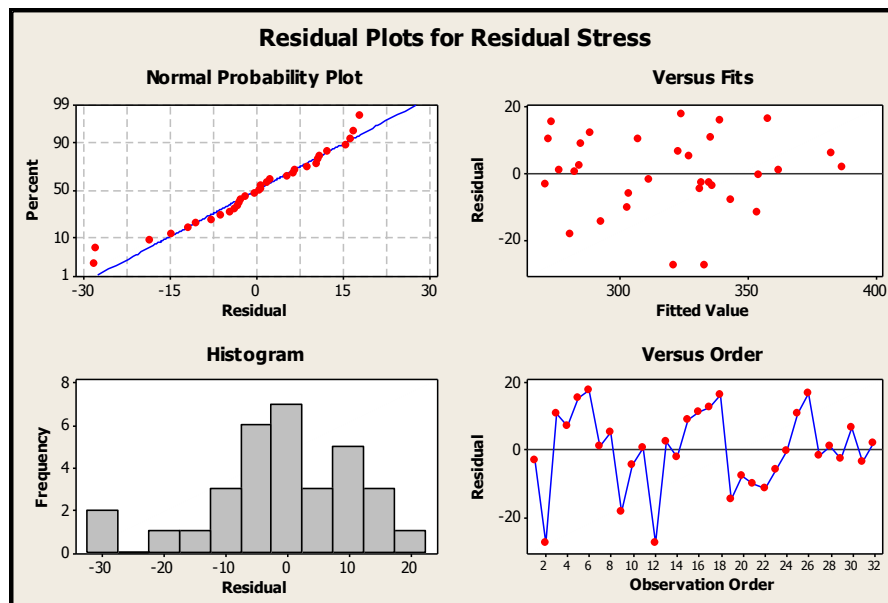


Figure B.2 Residual plots for response Residual Stress

Appendix C: Multiple Nonlinear Regression Analysis

C.1 Regression Model for Response Temperature Using DataFit 9.0

Model Definition $Y = a + b * \ln(x_1) + c * x_2$

The fitted nonlinear model 1 is: $T = 1844.12 + 881.64 * \ln(H) - 683.56 * S$

Table C.1 Regression variable results

Variable	Value	Standard Error	t-ratio	Prob(t)
a	1844.12	28.277165	65.2160	0.0
b	881.64	38.577461	22.8538	0.0
c	-683.56	29.912504	-22.8521	0.0

Table C.2 Nonlinear regression summary statistics

Sum of Residuals	2.27 E-13
Average Residual	1.42 E-14
Residual Sum of Squares (Absolute)	13772.0889
Residual Sum of Squares (Relative)	13772.0889
Standard Error of the Estimate	32.5483
Coefficient of Multiple Determination (R^2)	0.9839
Proportion of Variance Explained	98.391 %
Adjusted Coefficient of Multiple Determination (R^2_{adj})	0.9814
Durbin-Watson Statistic	1.5535

Table C.3 Variance Analysis (ANOVA)

Source	DF	Sum of Squares	Mean Square	F Ratio	Prob(F)
Regression	2	842501.324	421250.662	397.634	0
Error	13	13772.088	1059.391		
Total	15	856273.413			

C.2 Regression Model for Response Residual Stress Using DataFit 9.0

Model Definition $Y = \exp(a * x_1 + b * x_2 + c * x_3 + d)$

The fitted nonlinear model is: $R = \exp(0.3486 * H + 0.0417 * S + 0.4689 * C + 5.1119)$

Table C.4 Regression variable results

Variable	Value	Standard Error	t-ratio	Prob(t)
a	0.3486	0.0434	8.020	0.0
b	0.0417	0.0251	1.661	0.1078
c	0.4689	0.0400	11.717	0.0
d	5.1119	0.0451	113.297	0.0

Table C.5 Nonlinear regression summary statistics

Sum of Residuals	0.1060
Average Residual	3.314 E-03
Residual Sum of Squares (Absolute)	4188.05
Residual Sum of Squares (Relative)	4188.05
Standard Error of the Estimate	12.230
Coefficient of Multiple Determination (R^2)	0.8879
Proportion of Variance Explained	88.79%
Adjusted Coefficient of Multiple Determination (R_{adj}^2)	0.8759
Durbin-Watson Statistic	1.5389

Table C.6 Variance Analysis (ANOVA)

Source	DF	Sum of Squares	Mean Square	F Ratio	Prob(F)
Regression	3	33205.0376	11068.345	73.99	0
Error	28	4188.0505	149.573		
Total	31	37393.0881			

Vita

Manthan Malde was born in Hyderabad, Andhra Pradesh, India, in 1983. He completed his schooling from Shree HanumanVyayam Shala High School, Hyderabad, India. He received his Intermediate degree from Little Flower Junior College, Hyderabad, India. He received the Bachelor of Engineering Degree in Mechanical Engineering from MVSR College of Engineering, Hyderabad, India, in 2006. He then joined the graduate program at Louisiana State University, Baton Rouge, in August, 2006. He is a candidate for the Master of Science degree in Industrial Engineering to be awarded at the commencement in December, 2009.